American Mineralogist, Volume 92, pages 1133–1147, 2007

Crystal chemistry of synthetic $Ca_2Al_3Si_3O_{12}OH$–$Sr_2Al_3Si_3O_{12}OH$ solid-solution series of zoisite and clinozoisite

G. Dörsam,[1,*] A. Liebscher,[1,2] B. Wunder,[2] G. Franz,[1] and M. Gottschalk[2]

[1]Technische Universität Berlin, Fachgebiet Mineralogie, ACK 9, Ackerstr. 76, D-13355 Berlin, Germany
[2]GeoForschungszentrum Potsdam Telegraphenberg 14473 Potsdam, Germany

Abstract

Coexisting solid-solution series of synthetic zoisite-(Sr) and clinozoisite-(Sr) were synthesized in a 1 *M* $(Ca,Sr)Cl_2$ solution at 2.0 GPa, 600 °C for 6 days in a piston cylinder press. Solid solutions were synthesized from $X_{Sr}^{Zo} = Sr/(Ca + Sr) = 0.06$ to 1 and $X_{Sr}^{Czo} = 0.08$ to 0.5 in zoisite and clinozoisite, respectively. The products were characterized with SEM, EMP, and powder-XRD. Zoisites form crystals up to 30 μm in size. Lattice parameters of zoisite increase linearly with increasing Sr content. For synthetic zoisite-(Sr) lattice parameters are $a = 16.3567(5)$ Å, $b = 5.5992(2)$ Å, $c = 10.2612(5)$ Å, and $V = 939.78(7)$ Å^3 in space group *Pnma*. Volume of clinozoisite ($P2_1/m$) increases with increasing X_{Sr}^{Czo}, but the lattice parameter *a* collapses, and *b*, *c*, and β have a discontinuity at $X_{Sr}^{Czo} \approx 0.25$. The decrease in angle β of clinozoisite results in compression of M3 and T3 polyhedra and increase of the A2 polyhedron. A1-O7 distance of 2.12 Å in clinozoisite is extremely short at $X_{Sr}^{Czo} \approx 0.25$, but with further Sr incorporation on A2 this distance relaxes quickly to 2.24 Å, combined with a torsion of T3. In zoisite, Sr incorporation leads to an opposite movement of neighboring octahedral chains parallel *a* and causes changes in the linked T3, and angle O5-T3-O6 increases with X_{Sr} from 96.3 to 101°. The intra-crystalline distribution of Sr shows that A2 is the favored position and continuous incorporation on A1-position starts above $X_{Sr}^{Zo} \approx 0.35$ for zoisite and above $X_{Sr}^{Czo} \approx 0.45$ for clinozoisite.

Keywords: Zoisite, clinozoisite, strontium, synthesis, solid-solution series, hydrothermal, EMP data, XRD data

Introduction

Minerals of the epidote and lawsonite group are main constituents in metabasites and important carriers of trace elements such as Sr, Pb, and the rare earth elements. In mafic lawsonite blueschist more than 75% of the whole-rock Sr is located in lawsonite, and in eclogite about 99% in epidote minerals (Spandler et al. 2003). The element budget of Sr high-pressure rocks is therefore strongly controlled by these minerals.

During subduction of a metamorphosed oceanic crust, lawsonite and epidote minerals, which carry water into the deep subduction zone, will eventually dehydrate. To understand the role of Sr in the subduction process the distribution coefficients ($D_{Sr}^{mineral/fluid}$) are needed (Zack et al. 2002). The partitioning is generally controlled by pressure, temperature and bulk composition, i.e., a specific paragenesis. Brastad (1984) for example described Sr-metasomatism in an eclogite and partitioning of Sr between zoisite and clinozoisite, with a SrO-content of up to 7.4 wt% in zoisite and 4.7 wt% in clinozoisite. The importance of the epidote minerals as a carrier of Sr is underlined by the recent finding of niigataite [i.e. clinozoisite-(Sr) following the IMA-approved nomenclature of epidote-group minerals proposed by Armbruster et al. (2006)], which was found by Miyajima et al. (2003), in a coarse-grained prehnite-bearing rock from the Itoigawa-Ohmi district in central Japan.

* E-mail: guido.doersam@web.de

However, the ability to incorporate Sr into the minerals is first controlled by their structure, and to understand the solid-fluid behavior it is necessary to investigate the properties of the solid-solution series. Previous results (Liebscher and Franz 2004, Grapes and Hoskin 2004) imply that the complete Ca-Sr solid solution exists within the epidote mineral group. The epidotes exhibit, however, complex chemical and structural variations (Dollase 1968, 1971; Liebscher et al. 2002; Liebscher and Franz 2004), which may significantly influence the Ca-Sr partitioning. Both zoisite and clinozoisite [$A_2M_3O(SiO_4)(Si_2O_7)(OH)$ with A = Ca^{2+} and M = Al^{3+}] have two A positions A1 and A2 (Fig. 1a). In zoisite both positions are sevenfold-coordinated with mean distances (A1-O) = 2.46 Å, (A2-O) = 2.55 Å. In clinozoisite these distances are (A1-O) = 2.47 Å and (A2-O) = 2.57 Å for irregular sevenfold and eightfold coordination. Both structures have identical linkages of the A-polyhedra (Fig. 1b). Pairs of A2 share O2-O2 edges to form endless chains along **b** with the A1 polyhedra attached on the external sides by sharing faces involving O7 and two O3 atoms. The A2 position is larger in size and the most likely site for Sr, because the ionic radii are $^{VII}Ca^{2+}$ = 1.06 Å and $^{VII}Sr^{2+}$ = 1.21 Å (Shannon 1976).

Studies of structural changes in synthetic zoisite and clinozoisite were mainly focused on the octahedral sites M1 and M3. Giuli et al. (1999) report Al-Fe disorder on M-sites in synthetic epidotes, and the study of Nagashima and Akasaka (2004) shows structural changes in the synthetic piemontite-clinozoisite solid-

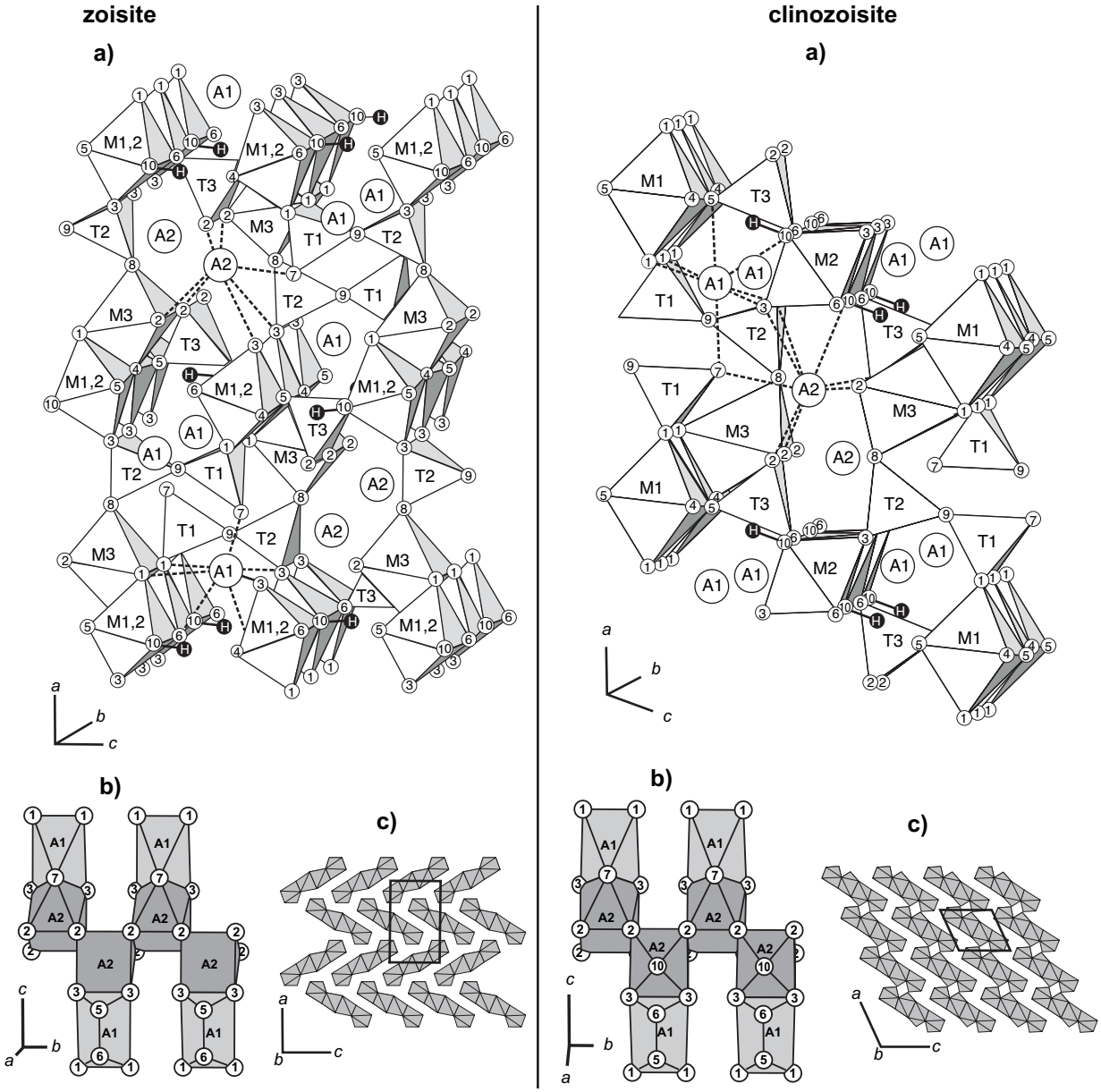

FIGURE 1. (**a**) Linkage of M-octahedra and T-tetrahedra in zoisite and clinozoisite. Dashed lines show the nearest oxygen neighbors of the A positions which form the A1 and A2 polyhedrons (redrawn after Dollase 1968; Liebscher and Franz 2004). (**b**) Linkage of A1 and A2 polyhedron in zoisite (left) and clinozoisite (right) in both structures is identical, A1 and A2 polyhedra share two O3 atoms and the O7 atom and are face-bonded. The A2 polyhedra are edge-bonded by O2-atoms and form chains along *b*. A1 is sevenfold-coordinated in both structures, but A2 in clinozoisite is furthermore strongly bonded to O10 and so eightfold-coordinated, what differs from the sevenfold-coordinated A2 in zoisite.

solution series. For synthetic zoisite, only Liebscher et al. (2002) has reported an isostructural phase transition within zoisite as a function of Fe^{3+}/Al content.

Bonazzi et al. (1990) investigated the substitution on the A-site in natural epidote. They analyzed two piemontite-(Sr) crystals with Sr contents (molar ratio) of X_{Sr} = Sr/(Ca + Sr) = 0.31 and 0.37 and found Sr only on the A2 site but additional substitution of Ca^{2+} by Mn^{2+} on the A1 site in one sample. The difference between the two, one with a combined substitution Ca-Mn and the other one without, are insufficient to explain the details of the Sr-Ca-substitution for the epidote mineral group.

Synthesis experiments of Akasaka et al. (2000) yielded the maximum strontium content of X_{Sr} = 0.55 for Ca-Sr solid solution of piemontite. At temperatures of 500–600 °C and pressures of 200–300 MPa they obtained the synthetic piemontite-(Sr) analog with crystals up to 25 μm in size. Unfortunately, their strontium content in piemontite varies strongly (ΔX_{Sr} = 0.1) within each sample. Solid-solution series from X_{Sr} = 0.09 to 0.55

were observed with variable amounts of manganese (X_{Mn} = 0.21 – 0.55). Error bars associated with the above mole fractions are too large and so the corresponding four sets of lattice parameters do not show a clear trend within the solid-solution series. No further details of structural changes for synthetic Ca-Sr solid solution of piemontite are given. Until now, no Mn- or Fe-free epidotes were synthesized to show the structural influence of Sr substitution on A1 and A2 sites over the whole solid-solution series.

To obtain both, information about the crystal chemistry of Ca-Sr solid solution of zoisite, clinozoisite, and crystal-fluid interactions, we synthesized Ca-Sr solid solutions at 2.0 GPa and 600 °C in a chloridic solution. Here we present data about the structural changes of zoisite and clinozoisite induced by Sr substitution and interpret the intra-crystalline partitioning of Sr and Ca between the A1 and A2 positions. Zoisite, clinozoisite-fluid interactions will be reported elsewhere.

Experimental techniques

Starting materials were oxide-hydroxide mixtures of SiO_2 (α-quartz, ignited, Fe-free p.a. Merck), γ-Al_2O_3 (Aldrich), $Ca(OH)_2$, and either $Sr(OH)_2 \cdot 8H_2O$ weighted in stoichiometric amounts of the desired $(Ca,Sr)_2Al_3Si_3O_{12}(OH)$ composition (Table 1) or synthetic mixture of α'-Sr_2SiO_4 and α-quartz with molar ratio of 1 (prepared from $SrCO_3$ plus quartz by igniting for ≈24 h at 1100 °C). Excess SiO_2 (3–10 mol%) was added to each run to account for preferred dissolution of SiO_2 in the fluid and to ensure quartz saturation. The Sr-Ca composition of the solid starting material (bulk) are given in molar fractions of Sr from $(Sr + Ca)_{solid}$, named X_{Sr}^{bulk} and range from X_{Sr}^{bulk} = 0.065 to 1.00, where $X_{Sr}^{bulk} = Sr/(Sr + Ca)$ in mol.

Following Zimmermann et al. (1996) a 1 *M* $(Ca,Sr)Cl_2$ aqueous solution with identical X_{Sr} as the solid starting material was added to overcome kinetic problems. The initial $(Sr + Ca)_{fluid}/[(Sr + Ca)_{fluid} + (Sr + Ca)_{solid}]$ ratios was varied between 0.025 and 0.157.

The starting mixtures of solids and fluid were sealed either in gold or platinum capsules of 10 to 13 × 2 mm with a wall thickness of 0.115 mm. Four capsules were run in a common assembly at a time. Experiments were performed at 600 °C and 2.0 GPa for 6 days, using a standard piston-cylinder apparatus with a NaCl cell and graphite furnace. The temperature was recorded with an accuracy of ±10 °C using a NiCrNi thermocouple placed closely adjoining the centre of the capsules. Pressure was controlled within ±50 MPa. The assembly was first pressurized to 1.8 GPa, then heated to 600 °C and finally pressurized to 2.0 GPa [except in the first runs (Pt2, Pt3, Pt4), which were overheated to 630 °C for about 2 min].

Samples were quenched to below 200 °C within less than 10 s by switching off the furnace current. After quenching, the capsules were cleaned, weight checked and opened in distilled H_2O. Solid run products were dried at 100 °C for 15 min. The solid run products were characterized by optical and scanning electron microscopy (SEM), electron microprobe (EMP) and powder X-ray diffraction with Rietveld refinement (XRD).

SEM and EMP

SEM images were obtained with a Hitachi-S2700 instrument. EMP analyses were performed on polished and carbon coated samples with a Cameca SX 50 microprobe using wavelength dispersive spectrometry (WDS) and the PAP correction program (Pouchou and Pichoir 1984). Acceleration voltage was 10 kV, beam current 15–20 nA, and beam diameter was 1 µm. Counting time for all elements was 16 s on the peak position and the background was measured for 8 s on of each side of the peak. The following lines and analyzer crystals were used: Sr*L*β(TAP), Si*K*β(TAP), Al*K*α(TAP), and Ca*K*α(PET). Standards employed were wollastonite (Si and Ca) and synthetic $SrAl_2Si_2O_8$ (Al and Sr).

XRD with Rietveld refinement

The run products were ground in an agate mortar for several minutes, diluted with Elmer's White glue and then evenly spread on a circular foil. During drying, the powder was stirred to minimize preferential orientation. The foil was covered with a second foil and placed into the transmission sample holder. Powder XRD patterns were recorded in transmission between 2Θ = 5 and 125° using a fully automated STOE STADI P diffractometer with Cu*K*α_1 radiation equipped with a primary monochromator and a 7° wide position sensitive detector (PSD). The normal-focus Cu X-ray tube was operated at 40 kV and 40 mA, using a take-off angle of 6°. We used a detector step size of 0.1° and a resolution of 2Θ = 0.01°. Phase proportions, unit cell and other structural parameters were refined using the GSAS software package for Rietveld refinement (Larson and Von Dreele 1987). The peaks were defined as pseudo-Voigt with variable Lorentzian character. The peak full-width at half maximum height was varied as a function of 2Θ using the parameters *U*, *V*, and *W* of Cagliotti et al. (1958). For the Lorentzian character the parameters *X* and *Y* were used. Because of the geometry of the STADIP diffractometer the recorded reflections were highly symmetric and no parameters describing the asymmetry

Table 1. Starting materials and initial weights of synthesis experiments; all runs at 600 °C, 2 GPa, 6 days

Run no.	Solids (mg)					Fluid (mg)	Initial distribution of Ca and Sr in solids and fluids		
	Synthetic mixture α'-Sr_2SiO_4 with α-quartz*	$Sr(OH)_2 \cdot 8H_2O$	SiO_2†	γ-Al_2O_3	$Ca(OH)_2$	1 *M* (Ca,Sr) Cl_2–sol.	X_{Sr}^{solid}	X_{Sr}^{fluid}	$(Sr + Ca)_{fluid}/(Sr + Ca)_{total}$
Au32	0.690	–	6.434	5.158	4.685	5.85	0.0625	0.0625	0.075
Au40	1.363	–	6.103	5.094	4.318	5.82	0.125	0.125	0.075
Au45	1.878	–	5.628	4.873	3.872	6.29	0.18	0.18	0.084
Pt4	–	3.507	5.232	4.036	2.933	5.27	0.25	0.25	0.084
Au31	2.731	–	5.613	5.103	3.707	5.78	0.25	0.25	0.074
Au34	3.501	–	5.340	5.110	3.367	5.93	0.32	0.32	0.076
Au35	3.211	–	4.898	4.687	3.088	10.77	0.32	0.32	0.139
Pt8	–	4.776	4.751	3.665	2.219	5.22	0.375	0.375	0.091
Au30	4.048		5.052	5.042	3.053	5.79	0.375	0.375	0.075
Au42	4.366		5.008	5.099	2.964	5.77	0.40	0.40	0.074
Pt3	–	6.769	5.05	3.895	1.887	5.33	0.50	0.50	0.087
Pt35		6.046	3.86	4.912	2.023	10.67	0.575	0.575	0.132
Pt36	5.672	–	3.081	4.239	1.540	11.36	0.625	0.625	0.157
Au43	7.112	–	4.017	5.112	1.733	6.05	0.65	0.65	0.076
Pt2	–	9.362	4.656	3.592	0.870	5.41	0.75	0.75	0.095
Au23‡	8.000	–	3.524	4.983	0.914	5.73	0.80	0.75	0.049
Au22‡	6.637	–	2.157	3.543	0.325	1.27	0.90	0.875	0.025
Au33	9.927	–	2.685	4.881	0.236	11.29	0.95	0.95	0.137
Au44	9.714	–	2.627	4.777	0.231	6.60	0.95	0.95	0.087
Au21	9.388	–	2.231	4.370	–	6.06	1.00	1.00	0.087

Note: All syntheses have about 3–10 mol% SiO_2 excess and $X_{Sr}^{solid} > X_{Sr}^{fluid}$.
* Synthetic mixture of α'-Sr_2SiO_4 and α-quartz with molar ratio of 1.
† p.a. Merck, α-SiO_2, ignited, Fe-free.
‡ Initial weight not stoichiometric.

of the peaks had to be used. To model the diffuse background from the amorphous foil and glue used for the preparation, the background was fitted with a real space correlation function. Zoisite was refined in space group *Pnma*, clinozoisite in space group $P2_1/m$. At lowest X_{Sr} (sample Au32) refinements started with the zoisite and clinozoisite structure data of Liebscher et al. (2002; their end-member zoisite I) and Dollase (1968), respectively. Toward higher X_{Sr} we successively used the refined structure models, obtained for zoisite and clinozoisite at lower X_{Sr}, as input data. Lawsonite, detected in runs with high X_{Sr}^{bulk}, was refined in space group $P2_1/m$, which is the monoclinic high-pressure form of lawsonite (Pawley and Allan 2001). In all experiments both structural parameters and weight fractions could be refined successfully. However, crystallographic data obtained from powder-XRD data become more inaccurate as the number of phases in the powder pattern increased. The refinements were performed in the following sequence: scale factor, background, zero-point correction, phase fractions, lattice parameter, preferred orientation, profile parameter Cagliotti *W* and Lorentz *X* atom parameter (not for hydrogen), site occupancy for the A1 and A2 position with fractions of Ca and Sr in zoisite and clinozoisite, and the A1 site occupancy with fractions of Ca and Sr in lawsonite, isotropic displacement parameters and remaining profile parameters Cagliotti *U* and *V* and Lorentz *Y*. We fixed the maximum site occupancy factor (SOF) for A1 and A2 to 1 for each and restricted the occupation for Ca and Sr atoms. X_{Sr}^{A1} values are the statistical site occupation with Sr on A1-position, $X_{Sr}^{A1} = Sr^{SOF} / (Sr^{SOF} + Ca^{SOF})$, X_{Sr}^{A2} on A2, respectively. Values are given for zoisite and clinozoisite in Table 2. The total fraction of Sr in zoisite is than $X_{Sr}^{zoisite} = (X_{Sr}^{A1} + X_{Sr}^{A2})/2$, with X_{Sr}^{A1} and X_{Sr}^{A2} of zoisite. The same counts for $X_{Sr}^{clinozoisite}$ with X_{Sr}^{A1} and X_{Sr}^{A2} of clinozoisite. When the refinements yielded negative values for X_{Sr}^{A1} (zoisite in Pt8; clinozoisite in Au45, Au34, and Au30), X_{Sr}^{A1} was constrained to zero.

Results

Description of run products

All experiments contain zoisite (18–100 wt%) plus additional phases clinozoisite, quartz, lawsonite, and strontianite (obtained from solid fluid separation), depending on X_{Sr}^{bulk} (Table 2). Zoisite forms idiomorphic to hypidiomorphic crystals with a width of 1–10 µm and a length of 10–30 µm (Figs. 2a–2c). The size of the zoisite crystals generally increases with increasing X_{Sr}^{bulk} (compare Figs. 2a and 2b). The large idiomorphic zoisite crystals show the typical orthorhombic morphology with faces (100), (001), (101), (210) (Fig. 2c; indexing made by comparison with crystal drawing in Tröger 1982). Clinozoisite from experiments with X_{Sr}^{bulk} = 0.0625 to 0.625 could not be positively identified by SEM and EMP, however, some of the prismatic crystals lack orthorhombic morphology and suggest monoclinic symmetry. Idiomorphic to hypidiomorphic lawsonite crystals, up to 10 µm in size, were detected in Sr-rich experiments (Fig. 2d). X_{Sr} varies between 0.82 and 1 in these crystals (details about the crystal chemistry of lawsonite solid solution will be published elsewhere). Small amounts of idiomorphic crystals of Ca-bearing strontianite were observed as 5–10 µm thick and 100 –600

Table 2. Results of phase identification and structure refinements (Rietveld analyses)

Run no.	Au32	Au40	Au45	Pt4	Au31	Au35	Au34	Pt8	Au30
X_{Sr}^{bulk}	0.0625	0.125	0.180	0.250	0.250	0.320	0.320	0.375	0.375
Refined phase proportions (wt%)									
zoisite	45	65	53	100	48	38	56	18	58
clinozoisite	50	33	47		47	58	41	77	35
quartz	5	2	‡	‡	5	4	3	5	7
lawsonite									
strontianite									
Refined lattice parameters									
zoisite									
a (Å)	16.1941(3)	16.2023(4)	16.2100(3)	16.2384(5)	16.2278(3)	16.230(2)	16.2383(2)	16.2421(4)	16.2435(9)
b (Å)	5.5505(3)	5.5512(4)	5.5529(4)	5.5580(2)	5.5576(4)	5.5591((6)	5.5603(5)	5.561(1)	5.5592(3)
c (Å)	10.0483(8)	10.0589(8)	10.0695(9)	10.0877(5)	10.0893(8)	10.0968(5)	10.1019(5)	10.1128(3)	10.1083(7)
V (Å^3)	903.2(1)	904.7(2)	906.4(2)	910.5(1)	909.9(2)	911.0(2)	912.1(2)	913.5(3)	912.8(1)
clinozoisite									
a (Å)	8.8652(6)	8.8693(7)	8.8688(4)		8.8795(10)	8.8737(6)	8.8763(5)	8.8740(5)	8.8780(6)
b (Å)	5.5753(2)	5.5732(3)	5.5739(2)		5.5766(4)	5.5763(3)	5.5774(2)	5.5767(3)	5.5760(3)
c (Å)	10.1449(6)	10.1537(6)	10.1696(4)		10.1873(8)	10.2014(7)	10.2055(5)	10.2189(6)	10.2114(6)
β (°)	115.42(1)	115.33(1)	115.29(0)		115.19(1)	115.15(1)	115.12(0)	115.10(1)	115.06(1)
V (Å^3)	452.88(4)	453.66(4)	454.56(3)		456.48(6)	456.95(5)	457.47(4)	457.94(5)	457.92(4)
Refined Sr-Ca composition and Sr site occupancies									
zoisite									
X_{Sr}^{zo}	0.06(2)	0.13(2)	0.16(3)	0.22(1)	0.25(3)	0.27(4)	0.24(2)	0.33(3)	0.32(3)
X_{Sr}^{A1}	0.02(2)	0.04(2)	0.03(2)	0.03(1)	0.06(2)	0.00(3)	0.00(2)	0*	0.04(2)
X_{Sr}^{A2}	0.09(3)	0.22(2)	0.29(3)	0.40(1)	0.44(3)	0.54(4)	0.47(2)	0.62(5)	0.59(3)
clinozoisite									
X_{Sr}^{czo}	0.078(31)	0.119(33)	0.150(13)		0.233(40)	0.248(31)	0.248(14)	0.292(22)	0.304(15)
X_{Sr}^{A1}	0.029(29)	0.007(34)	0*		0.017(36)	0.034(29)	0*	0.058(18)	0*
X_{Sr}^{A2}	0.128(33)	0.232(32)	0.300(25)		0.465(44)	0.462(33)	0.496(27)	0.526(25)	0.609(30)
Calculated density *D* (g/cm^3)									
zoisite	3.38	3.43	3.44	3.47	3.49	3.50	3.47	3.53	3.53
clinozoisite	3.39	3.41	3.42		3.47	3.47	3.47	3.50	3.50
Molar volume *V* (cm^3/mol)									
zoisite	136.10(2)	136.23(3)	136.49(3)	137.11(2)	137.02(3)	137.18(3)	137.35(3)	137.56(5)	137.45(2)
clinozoisite	136.39(1)	136.63(1)	136.90(1)		137.48(2)	137.62(2)	137.78(1)	137.92(2)	137.91(1)
Refinement statistics									
(I_{Zo}† – I_{Back})	5800	3629	4622	4308	4696	4634	3674	6586	2381
R_{wp}	0.0435	0.0523	0.0411	0.0605	0.0443	0.0436	0.0467	0.0396	0.0612
χ^2	1.54	1.17	1.47	1.19	1.55	1.30	1.26	1.21	1.16
DWd	1.022	1.314	1.058	1.310	1.004	1.182	1.222	1.270	1.318
R (F^2)	0.0342	0.0395	0.0507	0.0398	0.0403	0.0405	0.0367	0.0488	0.0422

* Not refined, fixed at $X_{Sr}^{A1} = 0$.
† Intensity of zoisite peak (013).
‡ Quartz present according to EMP/SEM analyses.

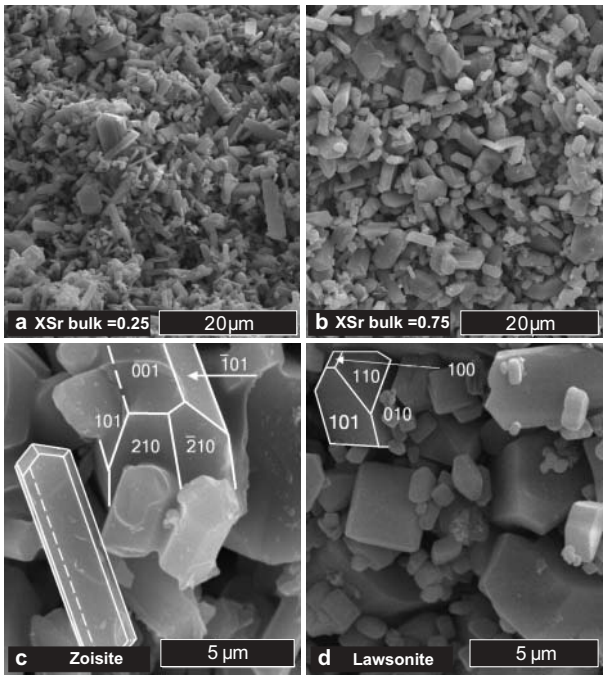

FIGURE 2. SEM-images of run products; (**a**) and (**b**) (runs Pt4 and Pt2, respectively) show the increase of crystal size with increasing X_{Sr}^{bulk}; (**c**) (run Pt3) shows idiomorphic crystals of zoisite; (**d**) shows lawsonite (run Au33).

µm long transparent prismatic needles. Zoisite and clinozoisite solid solutions were found to be homogeneous with respect to Ca/Sr within each individual experiment and single grain. X_{Sr}-content as determined by EMP (Table 3) indicates a composition substantially identical for zoisite and clinozoisite within the error limits of the microprobe analyses and is generally less than X_{Sr}^{bulk}, which is consistent with the preferential fractionation of Sr over Ca into the fluid and above $X_{Sr}^{bulk} > 0.5$ into lawsonite.

Powder X-ray diffraction with Rietveld refinement

XRD analysis confirmed the EMP data and indicated a similar composition for zoisite and clinozoisite within each individual experiment. However, based on the XRD data, Sr is possibly slightly preferred in the zoisite structure ($X_{Sr}^{Czo} = 0.93 \cdot X_{Sr}^{Zo}$; Fig. 3a, Table 2). To check for consistency of the analytical data, we plotted X_{Sr}^{Zo} as determined by EMP vs. X_{Sr}^{Zo} as determined by XRD (Fig. 3b). For those experiments that lack clinozoisite [i.e., in which $X_{Sr(EMP)} = X_{Sr}^{Zo}$] the data show an almost perfect linear cor-

TABLE 2. —*Extended*

Au42	Pt3	Pt35	Pt36	Au43	Pt2	Au23	Au22	Au33	Au44	Au21
0.400	0.500	0.575	0.600	0.650	0.750	0.750	0.875	0.950	0.950	1.000
41	98	26	95	33	92	69	59	56	76	81
58		55		40						
1	2	3	5	6	‡	4	31	2	2	7
		16		18		23	4	39	21	9
		1		3	7	2	6	3	1	3
16.253(5)	16.2798(7)	16.276(3)	16.2864(8)	16.284(2)	16.3048(7)	16.3095(8)	16.3229(1)	16.3432(8)	16.3376(5)	16.3548(1)
5.5630(5)	5.5676(2)	5.5694(9)	5.5719(3)	5.5741(5)	5.5769(2)	5.5814(2)	5.5871(3)	5.5943(3)	5.5936(2)	5.5985(1)
10.1196(2)	10.1388(6)	10.1463(2)	10.1606(5)	10.166(1)	10.1819(5)	10.1907(5)	10.2132(5)	10.2378(5)	10.2407(5)	10.2600(1)
915.1(2)	919.0(1)	919.7(3)	922.0(1)	922.8(2)	925.84(9)	927.6(1)	931.4(1)	936.0(1)	935.87(9)	939.43(1)
8.8796(5)		8.8871(16)		8.8923(2)						
5.5790(3)		5.5828(7)		5.5844(1)						
10.2257(6)		10.2452(14)		10.2585(2)						
115.06(0)		114.97(1)		114.99(0)						
458.89(5)		460.80(12)		461.70(5)						
0.37(3)	0.42(1)	0.51(3)	0.52(1)	0.55(3)	0.63(2)	0.66(4)	0.77(2)	0.86(2)	0.87(2)	1
0.09(3)	0.13(1)	0.18(3)	0.20(1)	0.19(3)	0.38(1)	0.41(3)	0.61(2)	0.76(2)	0.82(2)	1
0.67(3)	0.72(1)	0.84(3)	0.84(1)	0.82(4)	0.89(2)	0.92(4)	0.93(3)	0.96(2)	0.92(2)	1
0.349(27)		0.458(64)		0.513(40)						
0.001(26)		0.064(58)		0.148(37)						
0.698(28)		0.851(71)		0.878(43)						
3.55	3.57	3.63	3.63	3.65	3.69	3.70	3.76	3.80	3.81	3.88
3.53		3.59		3.62						
137.80(3)	138.39(2)	138.49(5)	138.84(2)	138.96(3)	139.42(1)	139.68(2)	140.25(2)	140.95(2)	140.93(2)	141.46(2)
138.20(2)		138.78(4)		139.05(2)						
4200	3607	4549	5927	4756	5757	2378	4424	4265	5376	3597
0.0538	0.0712	0.0498	0.0605	0.0518	0.0521	0.0419	0.0457	0.0646	0.0570	0.0744
1.29	1.21	1.43	1.23	1.22	1.44	1.07	1.19	1.23	1.14	1.08
1.216	1.296	1.125	1.27	1.269	1.072	1.436	1.335	1.227	1.372	1.461
0.0409	0.0388	0.0383	0.0369	0.0281	0.0504	0.0641	0.0474	0.0330	0.0330	0.0430

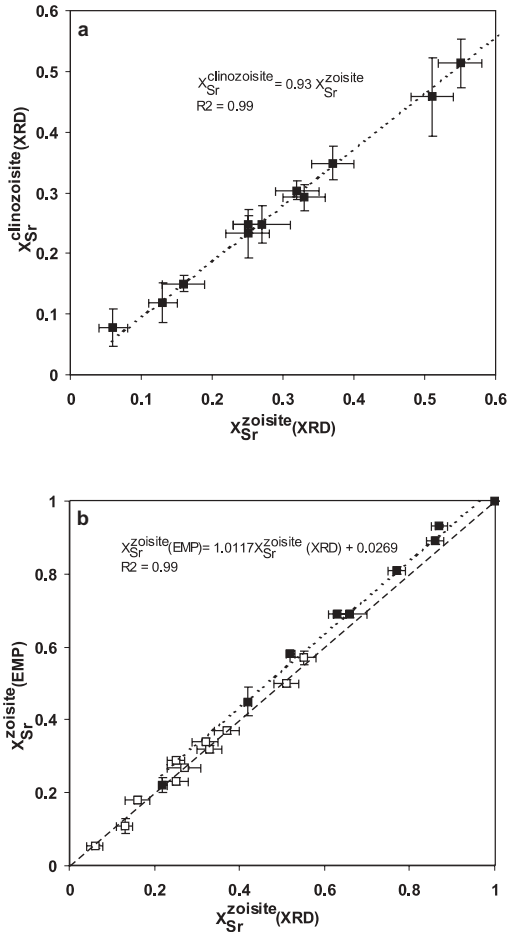

▲**FIGURE 3.** (**a**) $X_{Sr}^{clinozoisite}$ as a function of $X_{Sr}^{zoisite}$, based on XRD data in the range of X_{Sr} = 0.06 to X_{Sr} = 0.55; (**b**) comparison of X_{Sr} values of zoisite for the whole range $X_{Sr} \leq 1.0$, obtained from X-ray diffraction with EMP-data. Open squares represent EMP measurements of samples where zoisite and clinozoisite coexist, filled squares represent samples where only zoisite is present. Dotted line is the regression line for zoisite analyses, dashed line is the 1:1 reference line.

relation [$X_{Sr(EMP)}^{Zo} = 1.01\ X_{Sr(XRD)}^{Zo}$] and support the reliability of the compositions determined by XRD. In all other experiments X_{Sr} as determined by EMP is slightly below the correlation defined by the zoisite data. It must be left open whether the difference between the two data sets, one for zoisite only and the other one for zoisite plus clinozoisite (indistinguishable by EMP) is real or within error limits. Therefore, we will only refer to X_{Sr}^{Zo} and X_{Sr}^{Czo} as determined by XRD in the following.

Within the zoisite solid-solution series, the refined lattice parameter (Fig. 4) shows a linear trend as a function of X_{Sr}^{Zo} (Table 4) and the atom coordinates (Table 5a) display several changes. A selection of the data is shown in Figures 5a–5h (other data see Table A1[1]; the fractional coordinates of M3 and O1 behave similarly as M1). The lattice parameter of clinozoisite was monitored up to $X_{Sr}^{Czo} \approx 0.5$ (Fig. 6). Several significant changes are visible in atomic fractions of clinozoisite (Table 6a, a selection of the data is shown in Figs. 7a–7h). Within analytical precision the data indicate nearly identical intracrystalline Ca-Sr partitioning in zoisite and clinozoisite with a strong preference of Sr for A2; i.e., up to $X_{Sr} \approx 0.35$, Sr is almost exclusively incorporated on A2 with $X_{Sr}^{A1} < 0.06$ (Fig. 8a). Significant amounts of Sr on A1 (i.e., $X_{Sr}^{A1} > \sim 0.2$) are only observed for $X_{Sr}^{A2} > \sim 0.8$ in zoisite and clinozoisite (Fig. 8b).

[1] Deposit item AM-07-023, Tables 5b and 6b and Appendix Tables 1–8. Deposit items are available two ways: For a paper copy contact the Business Office of the Mineralogical Society of America (see inside front cover of recent issue) for price information. For an electronic copy visit the MSA web site at http://www.minsocam.org, go to the American Mineralogist Contents, find the table of contents for the specific volume/issue wanted, and then click on the deposit link there.

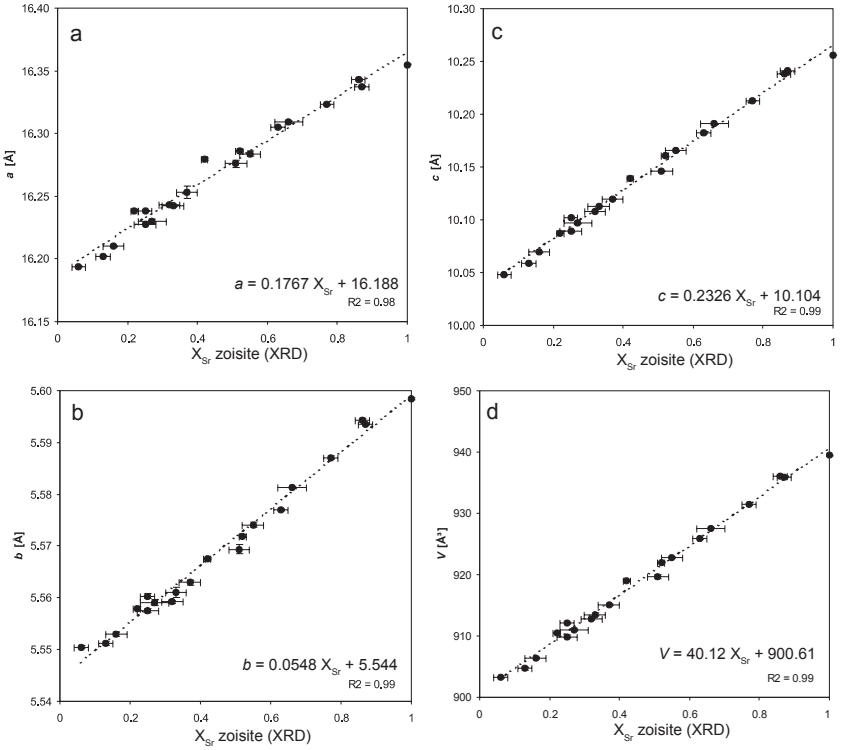

►**FIGURE 4.** (**a–d**) Variation of Ca-Sr zoisite lattice parameters as a function of X_{Sr}.

Discussion

The excess of SiO_2 in the starting composition is visible as quartz in the XRD pattern and/or in the EMP analysis. Therefore, quartz saturation is confirmed for all runs. According to the compilation of experimental data and thermodynamic properties of zoisite and clinozoisite in the CASH-CFASH system (Gottschalk 2004, and references therein), zoisite is at the given conditions the stable phase and remains stable at higher *P* and *T* in contrast to clinozoisite. Therefore, the presence of clinozoisite in all runs for $X_{Sr}^{bulk} < 0.65$ was unexpected. It is unlikely that the coexistence of synthetic zoiste and clinozoisite represents stable conditions, because in the pure CASH-system, the equilibrium between zoisite and clinozoisite lies below 200 °C, and in our experiments at 600 °C even for small X_{Sr}^{bulk} both phases were found. Thus, the run products in our experiments were probably not formed in a two-phase field where both Sr-bearing zoisite and clinozoisite are stable. Sr-bearing clinozoisite is therefore interpreted as a metastable run product. The coexistence of clinozoisite next to zoisite was not observed in a few runs (Pt4, Pt3, Pt2, and Pt36; Table 2). Pt2, Pt3, and Pt4 were set together in one run, which were overheated for about two minutes above 630 °C. For this special case we speculate that this temporary increase in temperature might have caused the elimination of metastable clinozoisite. Despite the fact that clinozoisite is metastable, the systematic behavior of the Ca-Sr distribution, both between zoisite and clinozoisite, and the intracrystalline distribution on the A sites in the phases indicates a metastable equilibrium.

In Sr-rich run products a Ca-Sr solid solution of lawsonite was found besides zoisite and clinozoisite, detected both via XRD and EMP. Experimental subsolidus studies on epidote minerals in the CASH system (see summary in Poli and Schmidt 2004) show that the stability limit of lawsonite + grossular ↔ zoisite + quartz + vapor at 2 GPa is at about 500 °C. Assuming that the synthesis of lawsonite represents conditions near equilibrium, the occurrence above the stability limit of pure Ca-bearing lawsonite indicates an increase in the thermal stability and thus a preferred Sr-incorporation into lawsonite.

Lattice parameters

The change of lattice parameters along the Ca-Sr solid-solution series in zoisite and clinozoisite is the sum of all structural changes caused by Sr incorporation on A1 and A2 positions at the constant run conditions. The strong increase in *c* with increasing X_{Sr} for clinozoisite and zoisite is related to the distance O2-O8 across the A2 polyhedra. It increases with X_{Sr}^{Zo} in zoisite from 3.55 to 3.78 Å, in clinozoisite from 3.41 to 3.70 Å at $X_{Sr}^{Czo} = 0.513$,

Table 3. Chemical composition of synthetic $(Ca,Sr)_2Al_3Si_3O_{12}(OH)$ solid solutions (averages of electron microprobe analyses)

Run no.	Au32	Au40	Au45	Pt4	Au31	Au34	Au35	Pt8	Au30	Au42
X_{Sr}^{bulk}*	0.0625	0.125	0.180	0.250	0.250	0.320	0.320	0.375	0.375	0.400
n†	35	18	6	11	14	16	13	10	22	17
SiO_2	38.85(63)	36.98(79)	37.69(50)	38.00(28)	36.36(122)	36.90(54)	37.33(31)	37.61(36)	35.92(90)	37.15(77)
Al_2O_3	33.37(65)	31.53(82)	32.29(27)	32.24(29)	30.71(102)	31.07(51)	31.65(33)	32.06(29)	30.25(90)	31.56(41)
CaO	22.21(35)	20.27(54)	19.24(16)	18.18(54)	17.36(60)	16.14(40)	16.83(18)	15.73(26)	14.65(42)	14.44(34)
SrO	2.28(17)	4.69(20)	7.55(33)	9.64(66)	9.39(33)	12.31(40)	11.47(26)	13.98(33)	14.13(42)	15.75(46)
Total	96.71(147)	93.47(204)	96.77(62)	98.06(58)	93.82(297)	96.42(133)	97.28(91)	99.39(66)	94.95(249)	98.90(105)
Cations per 12.5 O atoms										
Si	3.00(2)	3.00(3)	2.99(2)	3.00(1)	3.01(2)	3.01(1)	3.00(1)	3.00(2)	3.01(2)	3.00(3)
Al	3.04(2)	3.01(3)	3.02(3)	3.00(1)	3.00(2)	2.99(1)	3.00(1)	3.01(2)	2.99(2)	3.01(3)
Ca	1.84(2)	1.76(2)	1.64(2)	1.54(4)	1.54(2)	1.41(2)	1.45(1)	1.34(2)	1.32(1)	1.25(2)
Sr	0.10(1)	0.22(1)	0.35(1)	0.44(3)	0.45(1)	0.58(2)	0.54(1)	0.65(1)	0.69(1)	0.74(3)
Ca + Sr	1.94(2)	1.98(2)	1.99(1)	1.98(1)	1.99(1)	1.99(1)	1.99(1)	1.99(1)	2.01(1)	1.99(1)
$X_{Sr}^{zoisite}$	0.053(4)	0.11(2)	0.18(1)	0.22(2)	0.23(1)	0.29(1)	0.269(2)	0.32(1)	0.34(1)	0.37(1)

Run no.	Pt3	Pt35	Pt36	Au43	Au23	Au22	Pt2	Au33	Au44	Au21
X_{Sr}^{bulk}*	0.500	0.575	0.625	0.650	0.750	0.875	0.750	0.950	0.950	1.000
n†	59	17	19	11	13	7	5	12	10	16
SiO_2	36.26(66)	35.46(69)	34.80(40)	36.05(19)	34.61(38)	32.83(61)	34.80(28)	33.06(62)	33.07(37)	33.04(28)
Al_2O_3	30.98(50)	29.89(69)	29.37(42)	30.32(30)	29.13(52)	27.44(52)	29.07(46)	27.80(61)	27.87(17)	27.97(21)
CaO	12.33(92)	10.83(27)	9.01(19)	9.38(43)	6.66(39)	3.79(18)	6.78(39)	2.23(16)	1.41(7)	0.05(4)
SrO	18.95(149)	20.02(55)	22.99(49)	23.42(69)	27.29(48)	30.85(84)	27.50(49)	34.01(60)	35.59(23)	37.93(37)
Total	98.52(137)	96.2(192)	96.18(125)	99.17(71)	97.69(105)	94.91(206)	98.15(67)	97.10(186)	97.94(65)	98.99(36)
Cations per 12.5 O atoms										
Si	2.99(2)	3.00(2)	3.01(1)	3.02(1)	3.01(2)	3.01(1)	3.02(1)	3.01(1)	3.01(2)	3.00(2)
Al	3.01(2)	3.02(2)	2.99(1)	2.99(1)	2.99(3)	2.97(1)	2.97(2)	2.98(1)	2.98(2)	3.00(2)
Ca	1.09(7)	0.99(2)	0.84(1)	0.84(4)	0.62(3)	0.37(1)	0.63(3)	0.22(1)	0.14(1)	0.00(0)
Sr	0.91(8)	0.99(2)	1.15(2)	1.14(3)	1.38(2)	1.64(1)	1.38(3)	1.79(2)	1.88(1)	2.00(2)
Ca + Sr	2.00(2)	1.98(2)	1.99(1)	1.98(1)	2.00(3)	2.01(1)	2.01(2)	2.01(1)	2.02(1)	2.00
$X_{Sr}^{zoisite}$	0.45(4)	0.50(1)	0.58(1)	0.57(2)	0.69(1)	0.81(1)	0.69(2)	0.89(1)	0.932(2)	1.00

* Based on starting composition, see Table 1.
† Number of point analyses.

Table 4. Zoisite and clinozoisite lattice parameters as function of X_{Sr}^{Zo}, X_{Sr}^{Czo}

	zoisite	clinozoisite	
parameter	$0 \le X_{Sr}^{zo} \le 1$	$X_{Sr}^{czo} \le 0.25$	$X_{Sr}^{czo} \ge 0.25$
a =	0.1767 X_{Sr}^{Zo} + 16.188 (Å)	0.0762 X_{Sr}^{Czo} + 8.8592 (Å)	0.0712 X_{Sr}^{Czo} + 8.8551 (Å)
b =	0.0548 X_{Sr}^{Zo} + 5.544 (Å)	0.0178 X_{Sr}^{Czo} + 5.5723 (Å)	0.0341 X_{Sr}^{Czo} + 5.5669 (Å)
c =	0.2326 X_{Sr}^{Zo} + 10.035 (Å)	0.3294 X_{Sr}^{Czo} + 10.1180 (Å)	0.2042 X_{Sr}^{Czo} + 10.1530 (Å)
β =		−1.59 X_{Sr}^{Czo} + 115.53 (°)	−0.61 X_{Sr}^{Czo} + 115.27 (°)
V =	40.12 X_{Sr}^{Zo} + 900.61 (Å^3)	26.06 X_{Sr}^{Czo} + 450.69 (Å^3)	17.83 X_{Sr}^{Czo} + 452.6 (Å^3)

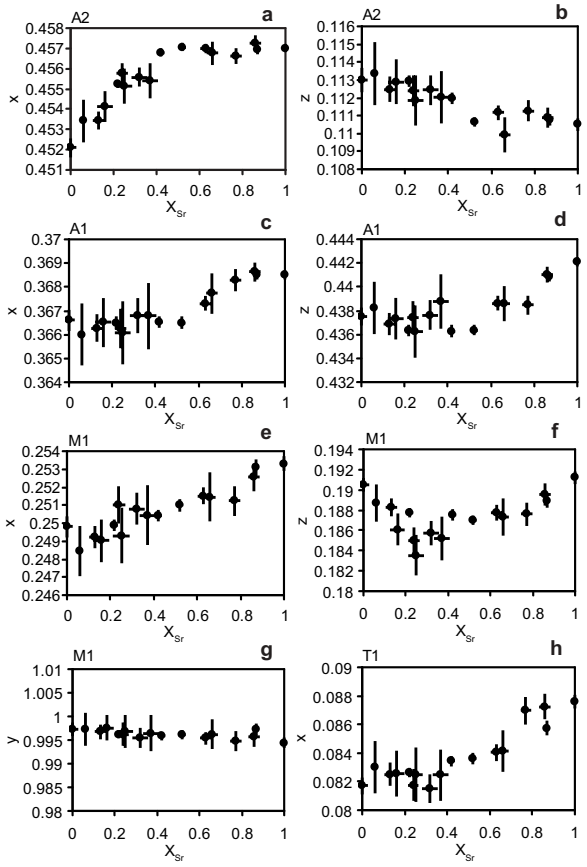

Figure 5. Changes in atomic positions for A1, A2, M1, and T1 in Ca-Sr zoisite with increasing X_{Sr}.

but is much lower in epidote (3.34 Å, Nozik et al. 1978) and in piemontite (3.32 Å, Dollase 1969).

Lattice parameter changes with X_{Sr} up to ≈ 0.25 of both zoisite and clinozoisite allows extrapolation of the trends to $X_{Sr} = 0$. The calculated lattice parameters are in good agreement with pure synthetic zoisite (Liebscher et al. 2002) and extrapolated pure clinozoisite based on the data of Carbonin and Molin (1980). The molar volumes of zoisite and clinozoisite increase similarly with X_{Sr} (Fig. 9). The cell volume of zoisite is about 3.3 Å^3 smaller than the doubled cell volume of clinozoisite. In the observed range, zoisite has a smaller molar volume corresponding to a higher density, and therefore analogous to the CASH-system Sr-bearing zoisite is the high-pressure phase.

Zoisite. The lattice parameters (Figs. 4a–4c) show that Sr incorporation in zoisite causes strong changes in *a* (slope $0.177 \cdot X_{Sr}$), *c* (slope $0.232 \cdot X_{Sr}$) but less in *b* (slope $0.055 \cdot X_{Sr}$), which differs from the trends found for Fe-Al substitution on M sites (Liebscher et al. 2002). Their data points in the range from $X_{Fe} = 0$ to ≈ 10 mol% Al_2Fe are split into two modifications zoisite I and zoisite II, with the transition point at ≈ 5 mol% Al_2Fe. Zoisite I and II of Liebscher et al. (2002) show a strong increase in *b* (slope $0.0816 \cdot Al_2Fe$) and steady decrease in *a* with increase of Al_2Fe. Changes in the M sites and changes in the A sites of zoisite cause very different, partly opposing effects in the lattice parameters with increasing substitution. Zoisite lattice parameters increase linearly over the entire compositional range $X_{Sr}^{Zo} = 0$ to 1 (Fig. 4, Table 4). Refined lattice parameters of the Sr end-member are $a^{Sr\text{-}Zo} = 16.3549(6)$ Å, $b^{Sr\text{-}Zo} = 5.5985(2)$ Å, $c^{Sr\text{-}Zo} = 10.2560(5)$ Å, and $V^{Sr\text{-}Zo} = 939.44(8)$ Å^3 (Table 2; run Au21).

Clinozoisite. In clinozoisite, lattice parameter *b* stays nearly unchanged in the observed range from $X_{Sr}^{Czo} = 0$ to 0.5 (small slope $0.018 \cdot X_{Sr}$ for $X_{Sr} < 0.25$, $0.034 \cdot X_{Sr}$ for $X_{Sr} > 0.25$). The incorporated larger Sr^{2+} ion therefore forces the structure to expand more in a and c direction. The variable monoclinic angle β decreases with X_{Sr}^{Czo} and reaches β = 114.99° at $X_{Sr} = 0.513$ (Fig. 6). The kink in the clinozoisite lattice parameters *b*, *c*, and β at $X_{Sr}^{Czo} \approx 0.25$ is combined with a sudden decrease in *a* and *V*. Decrease in β is typical for REE-bearing epidote minerals allanite and dissakisite (Dollase 1971; Bonazzi et al. 1996; Lavina et al. 2006), but our data are clear evidence that it is independent of substitutions by Mn^{2+}, Mg^{2+}, Fe^{2+} for Al^{3+} on M-sites coupled with REE^{3+} for Ca^{2+} on A2, or even incorporation of smaller cations such as Fe^{2+}, Mn^{2+}, or Mg^{2+} on A1. Lattice parameter *b* variation within the clinozoisite- clinozoisite-(Sr) solid-solution series is very small compared to the solid-solution series of clinozoisite-piemontite or clinozoisite-epidote. In Figure 10, the X_{Sr} series is compared to the X_{Mn} series (Anastasiou and Langer 1977) and X_{Fe} series (Carbonin and Molin 1980; Bonazzi and Menchetti 1995). Additional points for clinozoisite-(Sr) (Miyajima et al. 2003) and piemontite-(Sr) (Bonazzi et al. 1990) represent a mixture of the Mn and Fe series. The data show that Sr incorporation on the A2 site influences the lattice parameters, mainly *b*, *c*, and β but less when Fe is present in the M sites. Additional Mn strongly influences *a*, *b*, and *c*, but β is strongly influenced by Sr.

Clinozoisite lattice parameters vary monotonously with X_{Sr}^{Czo} over the observed compositional range $X_{Sr}^{Czo} \leq 0.5$ (Fig. 6), but with a change in the slope (especially for angle β) at $X_{Sr}^{Czo} \approx 0.25$, which is outside analytical uncertainty. Extrapolation of the linear regression (Table 4) for $X_{Sr}^{Czo} \geq 0.25$ to $X_{Sr}^{Czo} = 1$ yields $a^{Sr\text{-}Czo} = 8.9263$ Å, $b^{Sr\text{-}Czo} = 5.601$ Å, $c^{Sr\text{-}Czo} = 10.3572$ Å, $\beta^{Sr\text{-}Czo} = 114.66°$, and $V^{Sr\text{-}Czo} = 470.43$ Å^3 for the hypothetical monoclinic end-member $Sr_2Al_3Si_3O_{12}(OH)$.

Sr distribution and changes in A-polyhedra

The expected preferred Sr incorporation on the larger A2 position in both phases is confirmed by the results of the Rietveld refinement and best visible in Figure 8a. The difference in polyhedron size between A1 and A2 in clinozoisite is somewhat bigger than that in zoisite over the observed range (distances are reported in Tables A1 and A5). We assume that this causes the beginning of the substitution on the A1 position for clinozoisite at $X_{Sr}^{Czo} \geq 0.45$ compared to zoisite at $X_{Sr}^{Zo} \geq 0.35$. Nevertheless, the size of the A1 and A2 polyhedra is also a function of pressure and temperature and the intra-crystalline distribution can change with changing *P-T* conditions in the synthesis. At higher temperatures we expect a shift of the trend line toward the $K_D = 1$ line (Fig. 8b).

Zoisite. We found no obvious explanation as to why the A1 position in zoisite starts to incorporate Sr at values of $X_{Sr}^{Zo} > 0.35$, but the effect of the incorporation is well visible in the atomic positions of several atoms. With increasing X_{Sr}^{Zo} the polyhedral volume of A1 increases from 19.49 to 21.37 (Å^3) and that of A2 from 23.06 to 25.14 (Å^3) [Polyhedron volume and quadratic

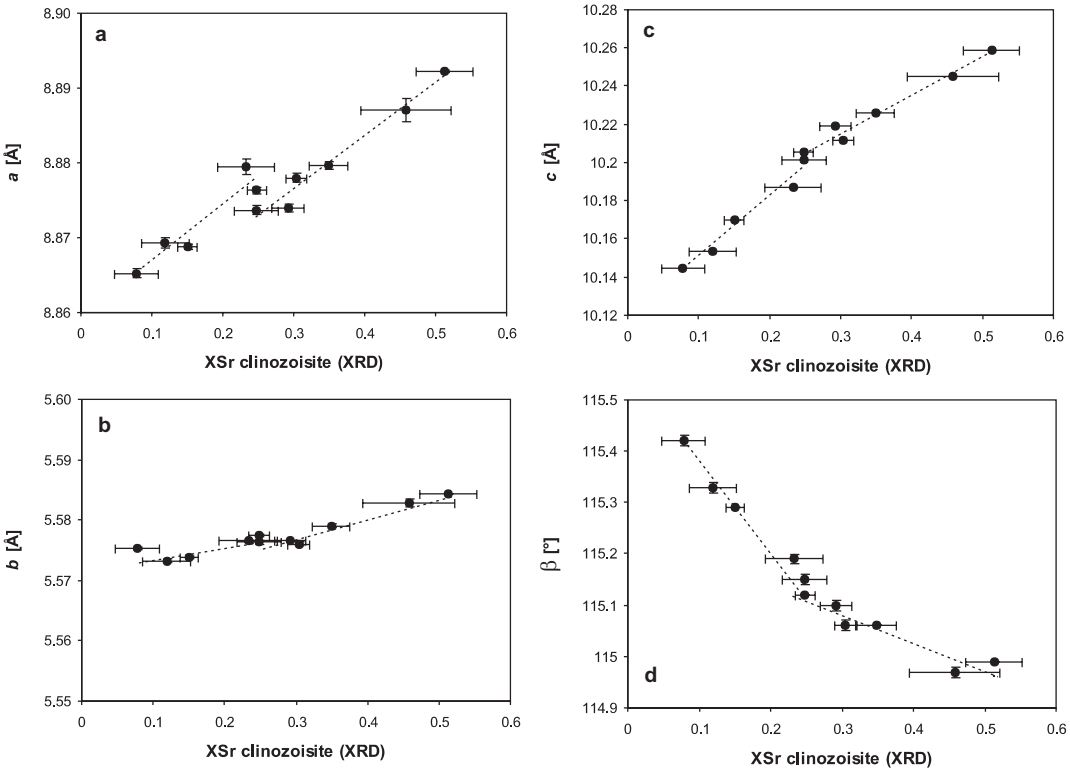

FIGURE 6. (**a–e**) Variation of Ca-Sr clinozoisite lattice parameters with X_{Sr} in the range X_{Sr} = 0.08 to X_{Sr} = 0.5. Lattice parameter *b* does not change significantly, whereas the angle β decreases. A discontinuity at $X_{Sr} \approx 0.25$ is most visible in lattice parameter *a* and angle β. Dotted lines are visual fits.

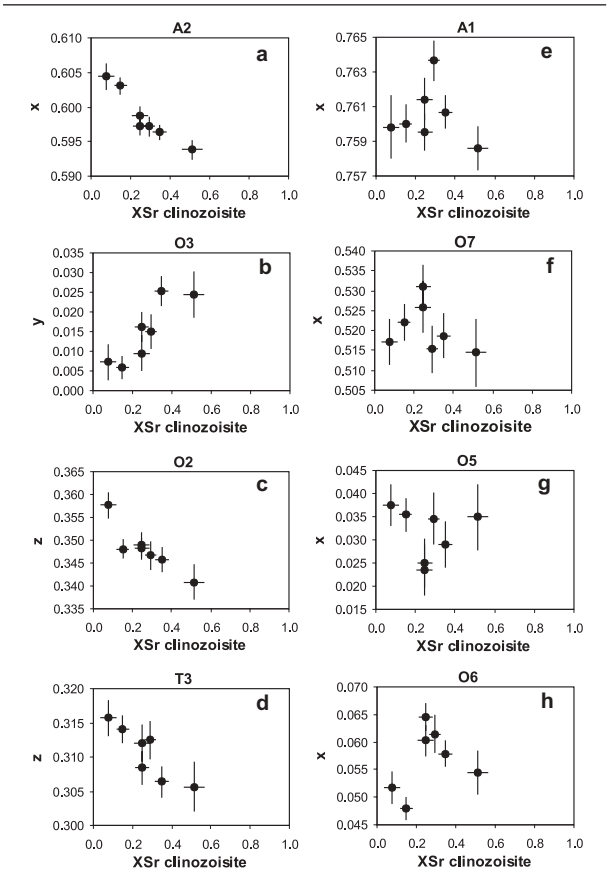

FIGURE 7. (**a–h**) Changes in atomic positions for atoms A1, A2, O2, O3, O5, O6, O7, and T3 in clinozoisite with increasing X_{Sr}.

elongation (Robinson et al. 1971) are reported in Table A4[1]. This increase behaves similar to the intracrystalline Sr distribution (Fig. 8a; see Table A1[1]) and independently of the result of the refined site fractions of A1 and A2. The observed increase of polyhedron volume A1 and A2 provides further information in support of Sr incorporation on these sites.

The differences in A1-O, A2-O bond length and the Sr incorporation at each position influence bond valences (see Table A3[1] bond valence parameter of Brown and Altermatt 1985) for A1 and A2. Calculations for $A1^{IX}$ and $A2^{X}$ show that bond valence values for A2 increase from 1.65 to 2.00 up to X_{Sr} = 0.35 and then stay constant, whereas the values for A1 position increase from 2 to 2.4.

Both A1 and A2 are strongly influenced by its nearest O atom O7, vertex of T1-tetrahedra. Within the whole solid-solution series the fraction of bond valences of O7 for A1 is 20–27%

TABLE 5A. Refined atomic positions of zoisite

Run no.				Au32	Au40	Au45	Pt4	Au31	Au34	Au30
X_{Sr}^{bulk}				0.06	0.13	0.16	0.22	0.25	0.24	0.32
Atom	M*	Wyk†	*x,y,z*							
A1	4	*c*	*x*	0.3660(13)	0.3663(5)	0.3665(10)	0.3665(2)	0.3661(13)	0.3664(8)	0.3668(7)
			y	¼	¼	¼	¼	¼	¼	¼
			z	0.438(2)	0.4369(8)	0.437(2)	0.4363(4)	0.436(2)	0.4373(13)	0.4376(11)
A2	4	*c*	*x*	0.4534(10)	0.4534(4)	0.4541(7)	0.4552(1)	0.4551(8)	0.4556(5)	0.4556(4)
			y	¼	¼	¼	¼	¼	¼	¼
			z	0.113(2)	0.1125(6)	0.1129(12)	0.1129(2)	0.1118(13)	0.1124(8)	0.1124(7)
Al1	8	*d*	*x*	0.2484(13)	0.2492(5)	0.2490(11)	0.2499(2)	0.2493(15)	0.2505(10)	0.2508(8)
			y	0.997(3)	0.9968(13)	0.998(2)	0.9961(5)	0.997(3)	0.996(2)	0.996(2)
			z	0.189(2)	0.1883(7)	0.1861(14)	0.1877(4)	0.184(2)	0.1852(12)	0.1858(11)
Al2	4	*c*	*x*	0.107(2)	0.1081(7)	0.106(2)	0.1066(3)	0.107(2)	0.1074(13)	0.1080(11)
			y	¾	¾	¾	¾	¾	¾	¾
			z	0.297(3)	0.295(1)	0.295(3)	0.2978(5)	0.294(3)	0.294(2)	0.293(2)
Si1	4	*c*	*x*	0.083(2)	0.0825(7)	0.083(2)	0.0826(3)	0.082(2)	0.0818(10)	0.0815(9)
			y	¼	¼	¼	¼	¼	¼	¼
			z	0.100(3)	0.1012(11)	0.101(2)	0.1037(5)	0.097(3)	0.100(2)	0.100(2)
Si2	4	*c*	*x*	0.413(2)	0.4114(7)	0.4125(14)	0.4113(3)	0.414(2)	0.4110(11)	0.4117(11)
			y	¾	¾	¾	¾	¾	¾	¾
			z	0.279(3)	0.2794(11)	0.278(2)	0.2818(5)	0.279(3)	0.278(2)	0.278(2)
Si3	4	*c*	*x*	0.158(2)	0.1589(7)	0.1597(13)	0.1606(3)	0.158(2)	0.1595(11)	0.1590(10)
			y	¼	¼	¼	¼	¼	¼	¼
			z	0.432(3)	0.4316(11)	0.432(2)	0.4316(5)	0.430(3)	0.432(2)	0.428(2)
O1	8	*d*	*x*	0.130(2)	0.1290(8)	0.130(2)	0.1296(3)	0.130(2)	0.1316(14)	0.1305(13)
			y	0.000(6)	0.002(3)	0.002(5)	0.0013(9)	0.005(6)	0.005(4)	0.006(3)
			z	0.148(3)	0.1476(12)	0.149(2)	0.1451(6)	0.145(3)	0.147(2)	0.146(2)
O2	8	*d*	*x*	0.105(2)	0.1029(8)	0.104(2)	0.1034(3)	0.105(2)	0.1049(14)	0.1048(12)
			y	0.012(6)	0.0120(2)	0.015(5)	0.0150(9)	0.019(6)	0.019(4)	0.020(3)
			z	0.427(4)	0.4260(15)	0.425(3)	0.4248(7)	0.424(4)	0.423(2)	0.422(2)
O3	8	*d*	*x*	0.359(2)	0.3598(8)	0.360(2)	0.3597(4)	0.360(2)	0.362(2)	0.3613(13)
			y	0.985(7)	0.990(3)	0.984(6)	0.9840(11)	0.989(7)	0.994(4)	0.988(4)
			z	0.244(3)	0.2428(13)	0.243(2)	0.2442(6)	0.241(3)	0.244(2)	0.242(2)
O4	4	*c*	*x*	0.220(3)	0.2201(13)	0.219(3)	0.2189(5)	0.223(4)	0.223(2)	0.223(2)
			y	¾	¾	¾	¾	¾	¾	¾
			z	0.299(5)	0.298(2)	0.297(4)	0.2954(9)	0.302(5)	0.295(3)	0.292(3)
O5	4	*c*	*x*	0.226(3)	0.2286(15)	0.228(3)	0.2276(5)	0.230(3)	0.229(2)	0.228(2)
			y	¼	¼	¼	¼	¼	¼	¼
			z	0.318(5)	0.315(2)	0.317(4)	0.3129(9)	0.317(5)	0.314(3)	0.313(3)
O6	4	*c*	*x*	0.274(3)	0.2739(13)	0.273(3)	0.2721(5)	0.273(3)	0.274(2)	0.272(2)
			y	¾	¾	¾	¾	¾	¾	¾
			z	0.065(5)	0.059(2)	0.065(4)	0.0578(9)	0.066(5)	0.064(3)	0.061(3)
O7	4	*c*	*x*	0.995(3)	0.9915(13)	0.994(3)	0.9932(5)	0.994(3)	0.994(2)	0.994(2)
			y	¼	¼	¼	¼	¼	¼	¼
			z	0.162(5)	0.161(2)	0.165(4)	0.1587(10)	0.161(5)	0.160(3)	0.162(3)
O8	4	*c*	*x*	0.006(4)	0.001(2)	0.004(3)	0.9990(6)	0.004(5)	0.002(2)	0.001(2)
			y	¾	¾	¾	¾	¾	¾	¾
			z	0.294(6)	0.293(2)	0.291(5)	0.2928(10)	0.294(6)	0.291(3)	0.289(3)
O9	4	*c*	*x*	0.421(3)	0.4205(13)	0.420(2)	0.4179(5)	0.419(3)	0.419(2)	0.420(2)
			y	¾	¾	¾	¾	¾	¾	¾
			z	0.436(6)	0.444(2)	0.447(5)	0.4438(11)	0.445(6)	0.441(4)	0.445(3)
O10	4	*c*	*x*	0.266(3)	0.2669(13)	0.267(3)	0.2678(5)	0.264(4)	0.267(2)	0.267(2)
			y	¼	¼	¼	¼	¼	¼	¼
			z	0.078(4)	0.078(2)	0.078(4)	0.0767(8)	0.077(5)	0.076(3)	0.078(3)

Note: Hydrogen (at position $x = 0.26$, $y = 0.25$, $z = 0.95$) was not refined. Refined U_{iso} values are given in deposited Table 5b[1].
* Multiplicity.
† Wyckoff letter.

and for A2 it is 16–23%. The influence of second order atoms, O10 and two O8 atoms for A2 and two O9 atoms for A1 stays below 5%. Therefore, the coordination numbers for both A1 and A2 are 7. In zoisite, the Ca-Sr substitution leads to displacement from the original positions A1 and A2 as a function of X_{Sr}. The mean bond lengths A1-O and A2-O increase. The substitution of Sr on the A2 position leads to an increase of the O3-O3 and O2-O2 distances, the edges of the A2 polyhedra. The O3-O3 edges are also edges of the A1-polyhedron, vertices of two neighbored M1,2-octahedra and T2-tetrahedra. The O2-O2 edge is further linked with M3-octahedra and T3-tetrahedra. Therefore, Sr incorporation on A2 can affect any polyhedra in the zoisite structure, which differs from that observed in clinozoisite (Figs. 11a, 11b, 12a, and 12b).

Clinozoisite. In clinozoisite, Sr incorporation leads to discontinuities in the changes of the lattice parameters and trends in atomic positions at $X_{Sr}^{Czo} \approx 0.25$. In the observed range, the volume of the A1 polyhedron increases with X_{Sr}^{Czo} from 18.14 to 19.41 (Å^3) and that of A2 from 28.13 to 30.26 (Å^3) (Polyhedron volume and quadratic elongation (Robinson et al. 1971) are reported in Table A8[1]). The volume of A1^{VII}-polyhedron jumps at $X_{Sr}^{Czo} \approx 0.25$ by about 1 (Å^3) and the increased total bond valence values for A1 falls strongly from 2.43 to 2.17 (Table A7[1]). The volume of the A2^{VIII}-polyhedron also shows a jump at this X_{Sr}^{Czo}-value and total bond valence values increase from 1.81 to 2.03. The jump causes an increase of the A1 and A2 polyhedra volumes and an

TABLE 5A.—*Extended*

Au42	Pt3	Pt36	Pt2	Au23	Au22	Au33	Au44	Au21
0.37	0.42	0.52	0.63	0.66	0.77	0.86	0.87	1
0.3668(13)	0.3665(2)	0.3665(2)	0.3673(3)	0.3677(3)	0.3683(4)	0.3686(3)	0.3685(2)	0.3685(1)
¼	¼	¼	¼	¼	¼	¼	¼	¼
0.439(2)	0.4363(4)	0.4363(3)	0.4386(5)	0.4386(5)	0.4385(7)	0.4410(5)	0.4408(3)	0.4421(2)
0.4554(8)	0.4568(1)	0.4571(1)	0.4570(2)	0.4568(2)	0.4566(3)	0.4573(3)	0.4569(1)	0.4570(1)
¼	¼	¼	¼	¼	¼	¼	¼	¼
0.1120(14)	0.1120(2)	0.1107(2)	0.1112(3)	0.1099(3)	0.1113(5)	0.1109(5)	0.1108(3)	0.1105(2)
0.250(2)	0.2504(2)	0.2510(3)	0.2515(4)	0.2515(5)	0.2512(7)	0.2525(7)	0.2531(3)	0.2533(2)
0.996(3)	0.9959(5)	0.9962(7)	0.9954(10)	0.9962(11)	0.995(2)	0.996(2)	0.9972(9)	0.9944(6)
0.185(2)	0.1875(4)	0.1870(3)	0.1877(6)	0.1873(6)	0.1876(10)	0.1896(9)	0.1889(5)	0.1912(3)
0.107(2)	0.1072(3)	0.1072(4)	0.1080(6)	0.1082(7)	0.1093(11)	0.1102(10)	0.1091(5)	0.1102(3)
¾	¾	¾	¾	¾	¾	¾	¾	¾
0.293(3)	0.2944(7)	0.2938(6)	0.2966(10)	0.2973(11)	0.295(2)	0.2966(15)	0.2976(8)	0.2977(5)
0.082(2)	0.0834(3)	0.0836(3)	0.0840(5)	0.0841(5)	0.0870(9)	0.0873(8)	0.0857(4)	0.0876(3)
¼	¼	¼	¼	¼	¼	¼	¼	¼
0.100(3)	0.1031(6)	0.1012(6)	0.1030(9)	0.0991(9)	0.103(2)	0.1054(14)	0.1034(8)	0.1057(5)
0.411(2)	0.4105(3)	0.4110(3)	0.4113(6)	0.4108(6)	0.4128(10)	0.4122(9)	0.4121(5)	0.4124(4)
¾	¾	¾	¾	¾	¾	¾	¾	¾
0.277(3)	0.2813(7)	0.2807(6)	0.2809(10)	0.2804(10)	0.282(2)	0.2831(15)	0.2836(8)	0.2823(5)
0.159(2)	0.1614(3)	0.1619(3)	0.1615(6)	0.1621(6)	0.1634(10)	0.1626(8)	0.1637(4)	0.1634(3)
¼	¼	¼	¼	¼	¼	¼	¼	¼
0.429(3)	0.4290(6)	0.4278(5)	0.4285(10)	0.4278(10)	0.427(2)	0.4291(14)	0.4304(7)	0.4311(5)
0.130(2)	0.1311(4)	0.1314(4)	0.1327(7)	0.1326(8)	0.1340(12)	0.1348(12)	0.1349(6)	0.1361(4)
0.002(6)	0.0014(10)	0.0026(11)	0.003(2)	0.003(2)	0.002(3)	0.000(3)	0.0019(14)	0.0040(9)
0.148(3)	0.1452(7)	0.1439(6)	0.1450(11)	0.1491(11)	0.148(2)	0.149(2)	0.1492(9)	0.1496(6)
0.105(3)	0.1038(4)	0.1060(4)	0.1058(7)	0.1077(8)	0.1077(11)	0.1072(11)	0.1073(6)	0.1071(4)
0.024(8)	0.0166(11)	0.0191(12)	0.018(2)	0.024(2)	0.024(3)	0.021(3)	0.0186(14)	0.0193(9)
0.420(5)	0.4225(8)	0.4210(7)	0.4214(12)	0.4176(12)	0.423(2)	0.421(2)	0.4214(9)	0.4188(6)
0.364(3)	0.3594(4)	0.3606(5)	0.3608(8)	0.3608(9)	0.3604(13)	0.3613(12)	0.3621(7)	0.3631(4)
0.987(8)	0.9849(12)	0.9845(14)	0.986(2)	0.982(2)	0.978(3)	0.983(3)	0.983(2)	0.9793(9)
0.244(3)	0.2449(7)	0.2413(6)	0.2434(11)	0.2441(12)	0.242(2)	0.242(2)	0.2417(9)	0.2409(6)
0.225(4)	0.2201(6)	0.2205(7)	0.2203(10)	0.2195(12)	0.223(2)	0.223(2)	0.2239(9)	0.2226(5)
¾	¾	¾	¾	¾	¾	¾	¾	¾
0.298(5)	0.2960(10)	0.2927(9)	0.2962(15)	0.295(2)	0.293(2)	0.297(2)	0.2994(12)	0.2952(8)
0.228(4)	0.2276(6)	0.2312(6)	0.2288(10)	0.2294(12)	0.228(2)	0.233(2)	0.2304(9)	0.2304(5)
¼	¼	¼	¼	¼	¼	¼	¼	¼
0.314(5)	0.3107(10)	0.3111(9)	0.3137(15)	0.311(2)	0.313(3)	0.313(2)	0.3106(12)	0.3132(8)
0.272(3)	0.2726(6)	0.2717(6)	0.2727(9)	0.2723(11)	0.270(2)	0.2753(14)	0.2741(8)	0.2762(5)
¾	¾	¾	¾	¾	¾	¾	¾	¾
0.070(5)	0.0549(10)	0.0569(9)	0.056(2)	0.063(2)	0.058(3)	0.058(2)	0.0586(13)	0.0588(8)
0.992(3)	0.9948(6)	0.9927(7)	0.9959(10)	0.9933(11)	0.997(2)	0.998(2)	0.9966(10)	0.0018(6)
¼	¼	¼	¼	¼	¼	¼	¼	¼
0.153(5)	0.1521(12)	0.1542(9)	0.157(2)	0.158(2)	0.155(3)	0.155(2)	0.1557(14)	0.1593(9)
0.002(4)	0.9985(7)	0.0028(8)	0.0006(12)	0.0050(13)	0.005(2)	0.004(2)	0.0050(10)	0.0056(5)
¾	¾	¾	¾	¾	¾	¾	¾	¾
0.291(5)	0.2914(11)	0.2905(10)	0.285(2)	0.290(2)	0.287(3)	0.286(2)	0.2838(14)	0.2839(9)
0.417(3)	0.4159(6)	0.4167(6)	0.4146(10)	0.4149(11)	0.414(2)	0.4159(14)	0.4158(8)	0.4146(5)
¾	¾	¾	¾	¾	¾	¾	¾	¾
0.434(5)	0.4403(12)	0.4445(11)	0.445(2)	0.451(2)	0.450(3)	0.445(3)	0.4472(14)	0.4503(9)
0.265(4)	0.2671(6)	0.2705(6)	0.2703(9)	0.2699(10)	0.273(2)	0.2743(14)	0.2721(8)	0.2742(5)
¼	¼	¼	¼	¼	¼	¼	¼	¼
0.075(6)	0.0755(11)	0.0756(9)	0.075(2)	0.0819(14)	0.080(2)	0.076(2)	0.0786(12)	0.0809(8)

increase in the atomic distance A1-O7. This distance is reduced with increasing X_{Sr}^{Czo} and reaches a minimum of 2.05 Å at $X_{Sr}^{Czo} \approx 0.25$ but jumps hereafter to 2.24 Å (Table A5[1]) with further Sr incorporation on A2. It is noteworthy that the bondings in A1 polyhedra run parallel a direction (A1-O7, A1-O5), or parallel the b-c plane (A1-O1, A1-O3), with exception of the bonding A1-O6. A decrease in angle β with incorporation of Sr on A2 increases so the A1-O6 bonding of the A1 polyhedra without a direct effect on the other A1-O bonds. Independently of the increase of *a* and *c*, or Sr incorporation, the decrease in β causes in general an increase in volume of the A2 polyhedron.

The fractions of O7 of the total A1 bond valences are 25 to 33% before and 23 to 25% after the jump. This means that the influence of the oxygen atoms, which surround the A1 position, are more equalized at $X_{Sr}^{Czo} > 0.25$. Because the solid-solution series ends at $X_{Sr}^{Czo} \approx 0.5$, it remains unclear if complete Sr substitution on A1 in clinozoisite is possible. Further A1-O distances and bond valence calculations are given in Tables A5 and A7[1].

Changes in M-octahedra. Only insignificant changes within the zoisite polyhedra M1, M2, M3, T1, and T2 were observed (see interatomic distances and angles, Tables A1 and A2[1]). The relaxation of the framework is characterized by a small displacement of the complete M1, M2 octahedral chain along *x* (Fig. 11a). The linkage T2-O8-M3 works thereby as a pin joint.

Because of the symmetry of zoisite, there is only one octahedral chain M1,2, neighbored by A2 and A1 polyhedra (Fig. 12a). This

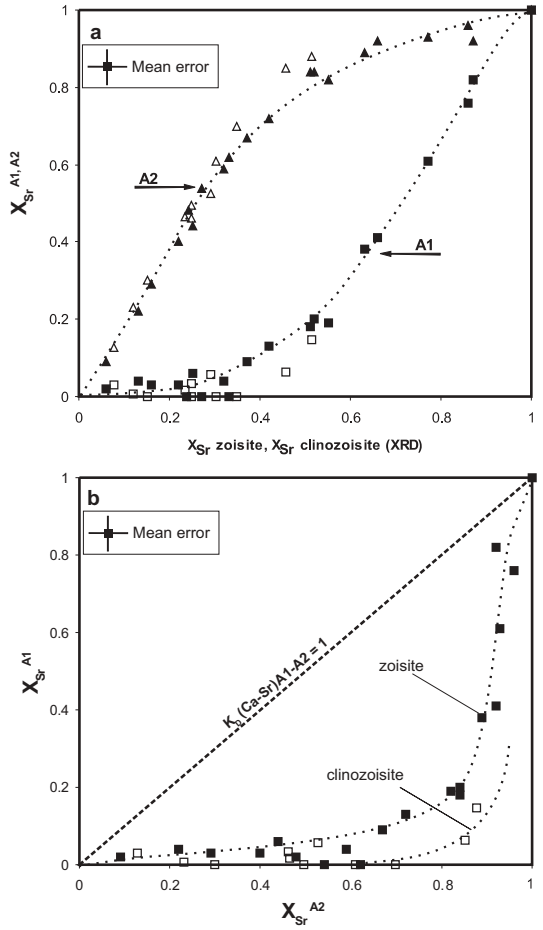

◄**FIGURE 8.** (**a**) Intracrystalline Sr-distribution on the A1- (squares) and A2-sites (triangles) for clinozoisite (open symbols) and zoisite (closed symbols); (**b**) X_{Sr} on A1 as a function of X_{Sr} on A2 showing preferred Sr-substitution on A2 position.

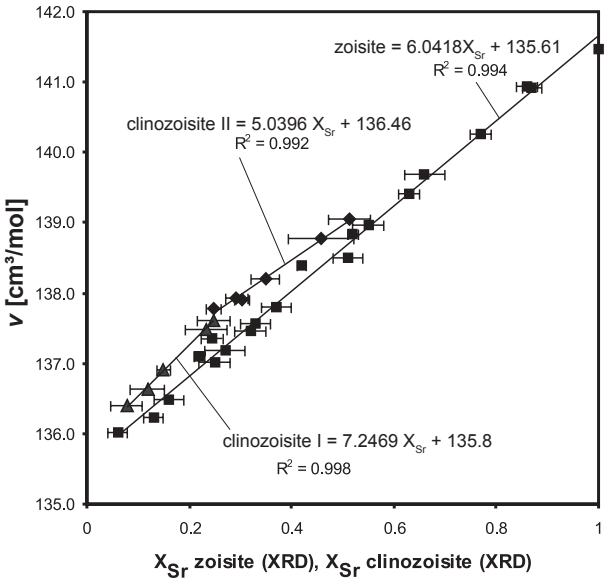

▲**FIGURE 9.** Variation of molar volume with X_{Sr} in zoisite (squares), clinozoisite with $X_{Sr} \leq 0.25$ (triangles), and clinozoisite with $X_{Sr} \geq 0.25$ (diamonds).

►**FIGURE 10.** Comparison of the variation in lattice parameters due to the Ca-Sr-substitution on A1 and A2 in clinozoisite (filled squares, this work), compared with Al-Fe-substitution in clinozoisite (open triangles, Carbonin and Molin 1980; Bonazzi and Menchetti 1995) and Al-Mn-substitution in piemontite (open circles, Anastasiou and Langer 1977; small open circles, Langer et al. 2002; cross, Nagashima et al. 2004) on the M-sites. Data points for niigataite (gray circle, Miyajima et al. 2003) and strontiopiemontite (gray square, Bonazzi et al. 1990) lie between the series.

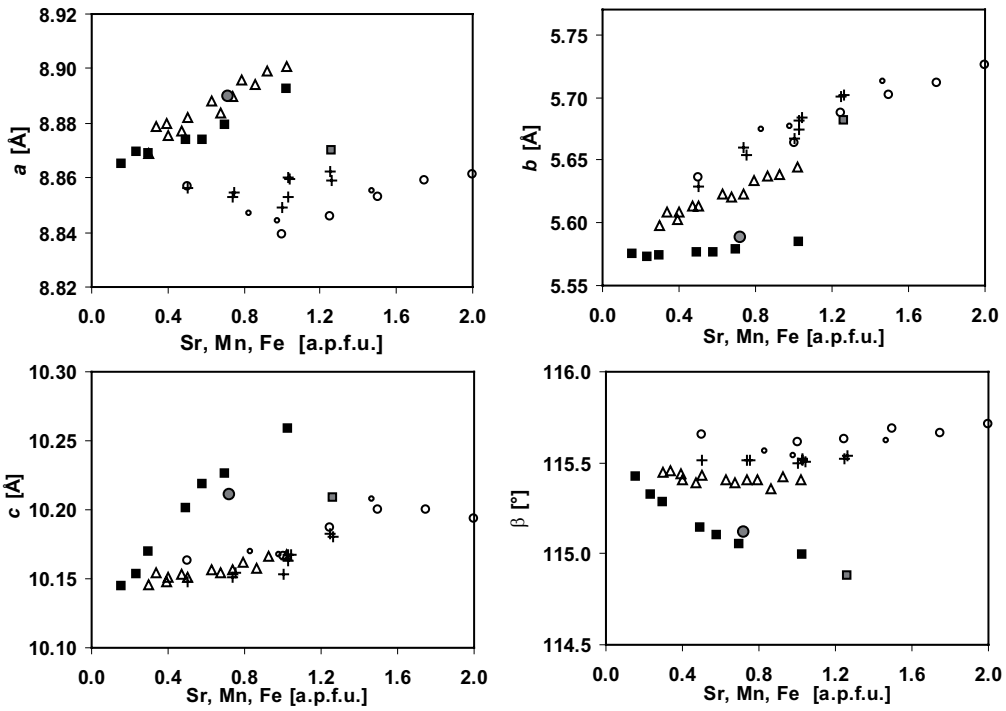

TABLE 6A. Refined atomic positions of clinozoisite

Run no.				Au32	Au45	Au31	Au35	Au34	Pt8	Au42	Pt35	Au43
X_{Sr}^{bulk}				0.078	0.15	0.233	0.248	0.248	0.292	0.37	0.458	0.513
Atom	M*	Wyk†	x, y, z									
A1	2	*e*	*x*	0.760(1)	0.760(2)	0.761(2)	0.761(1)	0.760(2)	0.764(1)	0.761(1)	0.755(1)	0.759(1)
			y	¾	¾	¾	¾	¾	¾	¾	¾	¾
			z	0.156(1)	0.159(2)	0.160(1)	0.159(1)	0.159(1)	0.159(1)	0.157(1)	0.155(1)	0.157(1)
A2	2	*e*	*x*	0.604(1)	0.603(1)	0.603(1)	0.599(1)	0.597(1)	0.597(1)	0.596(1)	0.593(1)	0.594(1)
			y	¾	¾	¾	¾	¾	¾	¾	¾	¾
			z	0.423(1)	0.422(1)	0.421(1)	0.422(1)	0.420(1)	0.421(1)	0.422(0)	0.420(1)	0.423(0)
Al1	2	*a*	*x*	0	0	0	0	0	0	0	0	0
			y	0	0	0	0	0	0	0	0	0
			z	0	0	0	0	0	0	0	0	0
Al2	2	*c*	*x*	0	0	0	0	0	0	0	0	0
			y	0	0	0	0	0	0	0	0	0
			z	½	½	½	½	½	½	½	½	½
Al3	2	*e*	*x*	0.286(1)	0.283(2)	0.269(2)	0.284(1)	0.287(2)	0.286(1)	0.286(1)	0.295(2)	0.289(2)
			y	¼	¼	¼	¼	¼	¼	¼	¼	¼
			z	0.224(1)	0.224(2)	0.216(1)	0.219(1)	0.216(2)	0.219(1)	0.219(1)	0.224(2)	0.216(1)
Si1	2	*e*	*x*	0.333(1)	0.338(2)	0.338(2)	0.338(1)	0.339(2)	0.337(1)	0.338(1)	0.334(2)	0.335(1)
			y	¾	¾	¾	¾	¾	¾	¾	¾	¾
			z	0.044(1)	0.039(2)	0.031(1)	0.042(1)	0.039(2)	0.046(1)	0.040(1)	0.038(1)	0.038(1)
Si2	2	*e*	*x*	0.679(1)	0.680(2)	0.675(2)	0.679(1)	0.677(2)	0.679(1)	0.680(1)	0.684(2)	0.679(2)
			y	¼	¼	¼	¼	¼	¼	¼	¼	¼
			z	0.277(1)	0.281(2)	0.281(1)	0.280(1)	0.279(2)	0.277(1)	0.280(1)	0.281(1)	0.278(1)
Si3	2	*e*	*x*	0.181(1)	0.177(2)	0.181(2)	0.179(1)	0.177(2)	0.180(1)	0.177(1)	0.170(2)	0.178(2)
			y	¾	¾	¾	¾	¾	¾	¾	¾	¾
			z	0.316(1)	0.314(2)	0.317(2)	0.312(1)	0.308(2)	0.312(1)	0.306(1)	0.307(1)	0.306(1)
O1	4	*f*	*x*	0.231(2)	0.239(3)	0.236(3)	0.234(2)	0.230(3)	0.237(1)	0.228(2)	0.242(2)	0.233(2)
			y	0.000(3)	0.002(5)	0.010(5)	0.002(3)	0.006(5)	0.996(3)	0.002(3)	0.015(3)	0.999(3)
			z	0.045(1)	0.049(2)	0.048(2)	0.047(2)	0.049(2)	0.048(1)	0.046(2)	0.054(2)	0.048(2)
O2	4	*f*	*x*	0.300(1)	0.301(2)	0.300(2)	0.298(1)	0.295(2)	0.296(1)	0.294(2)	0.284(2)	0.289(2)
			y	0.985(2)	0.980(3)	0.987(2)	0.982(2)	0.983(3)	0.986(2)	0.983(2)	0.983(2)	0.987(2)
			z	0.358(1)	0.348(2)	0.348(1)	0.349(1)	0.348(2)	0.347(1)	0.346(1)	0.345(2)	0.341(1)
O3	4	*f*	*x*	0.782(1)	0.782(2)	0.789(2)	0.781(2)	0.778(2)	0.789(2)	0.781(2)	0.781(3)	0.783(2)
			y	0.007(2)	0.006(3)	0.003(3)	0.010(2)	0.016(3)	0.015(2)	0.025(2)	0.014(2)	0.024(2)
			z	0.346(1)	0.346(2)	0.350(2)	0.347(1)	0.347(2)	0.349(1)	0.345(1)	0.348(2)	0.347(2)
O4	2	*e*	*x*	0.045(2)	0.044(4)	0.033(4)	0.048(2)	0.043(3)	0.059(2)	0.049(2)	0.041(3)	0.047(2)
			y	¼	¼	¼	¼	¼	¼	¼	¼	¼
			z	0.119(2)	0.124(3)	0.108(3)	0.129(2)	0.130(4)	0.129(2)	0.127(2)	0.123(2)	0.126(2)
O5	2	*e*	*x*	0.038(2)	0.035(4)	0.022(3)	0.023(2)	0.025(3)	0.035(2)	0.029(2)	0.035(4)	0.035(2)
			y	¾	¾	¾	¾	¾	¾	¾	¾	¾
			z	0.141(2)	0.137(4)	0.134(3)	0.142(2)	0.142(3)	0.148(2)	0.140(2)	0.142(3)	0.145(2)
O6	2	*e*	*x*	0.052(4)	0.048(7)	0.112(7)	0.060(4)	0.065(5)	0.061(2)	0.058(2)	0.055(4)	0.054(3)
			y	¾	¾	¾	¾	¾	¾	¾	¾	¾
			z	0.387(4)	0.394(6)	0.410(7)	0.397(3)	0.395(4)	0.395(2)	0.392(2)	0.396(3)	0.389(2)
O7	2	*e*	*x*	0.517(3)	0.522(5)	0.509(5)	0.526(3)	0.531(4)	0.515(2)	0.519(3)	0.556(4)	0.514(3)
			y	¾	¾	¾	¾	¾	¾	¾	¾	¾
			z	0.159(2)	0.165(4)	0.152(4)	0.166(3)	0.164(4)	0.167(2)	0.168(2)	0.176(3)	0.166(2)
O8	2	*e*	*x*	0.511(3)	0.524(5)	0.503(4)	0.505(3)	0.498(5)	0.504(3)	0.505(3)	0.508(4)	0.498(3)
			y	¼	¼	¼	¼	¼	¼	¼	¼	¼
			z	0.299(2)	0.318(4)	0.310(3)	0.303(2)	0.294(4)	0.299(2)	0.296(3)	0.299(3)	0.289(3)
O9	2	*e*	*x*	0.646(3)	0.646(5)	0.634(5)	0.653(3)	0.659(4)	0.658(3)	0.658(3)	0.667(3)	0.657(3)
			y	¼	¼	¼	¼	¼	¼	¼	¼	¼
			z	0.110(3)	0.117(5)	0.117(5)	0.116(3)	0.122(4)	0.117(2)	0.119(2)	0.118(3)	0.109(3)
O10	2	*e*	*x*	0.071(3)	0.079(6)	0.037(6)	0.070(3)	0.076(5)	0.069(3)	0.077(3)	0.064(4)	0.078(3)
			y	¼	¼	¼	¼	¼	¼	¼	¼	¼
			z	0.408(3)	0.424(6)	0.402(5)	0.428(3)	0.436(5)	0.424(2)	0.430(2)	0.415(3)	0.429(3)

Note: Hydrogen (at position $x = 0.046$, $y = 0.25$, $z = 0.341$) was not refined. Refined U_{iso} values are given in deposited Table 6b.
* Multiplicity.
† Wyckoff letter.

differs from the polyhedral arrangement in clinozoisite where we have two separate octahedron chains of M1 and M2. M2 is neighbored by A1 and A2 polyhedra, whereas M1 is only neighbored by the A1 polyhedron, and therefore not directly affected by changes in the A2 site (Fig. 12b). The laterally linked M3 octahedron on the M1 chain is only neighbored by A2 polyhedra.

With strong Sr-substitution on A2 but none on A1, the M2 and M3 polyhedra of clinozoisite are compressed and therefore show a volume decrease (see polyhedra volume, Table A8[1]). M1 increases in volume as long as a larger atom does not occupy A1. The volume decrease of M3 is unaffected by the entry of Sr on A1 and decreases further with X_{Sr} on A2. In contrast, with Sr entry on A1, M1 polyhedron volume decreases whereas M2 polyhedron volume increases.

With increasing X_{Sr} all three M polyhedra volume [at $X_{Sr}^{czo} = 0.08$ polyhedra volumes are M1 = 8.52(Å^3), M2 = 9.62 (Å^3), M3 = 10.05(Å^3)] converge to 9.30 (Å^3). In general the convergence of the M-polyhedra sizes should have a positive effect on structure stability when the M sites are occupied by one atom type (Al^{3+}).

Substitution on the M-sites changes directly the M1 and M2 octahedral chains. In particular, the average M1-O4, M1-O5, and the M1 distances of piemontite (Nagashima and Akasaka 2004) are

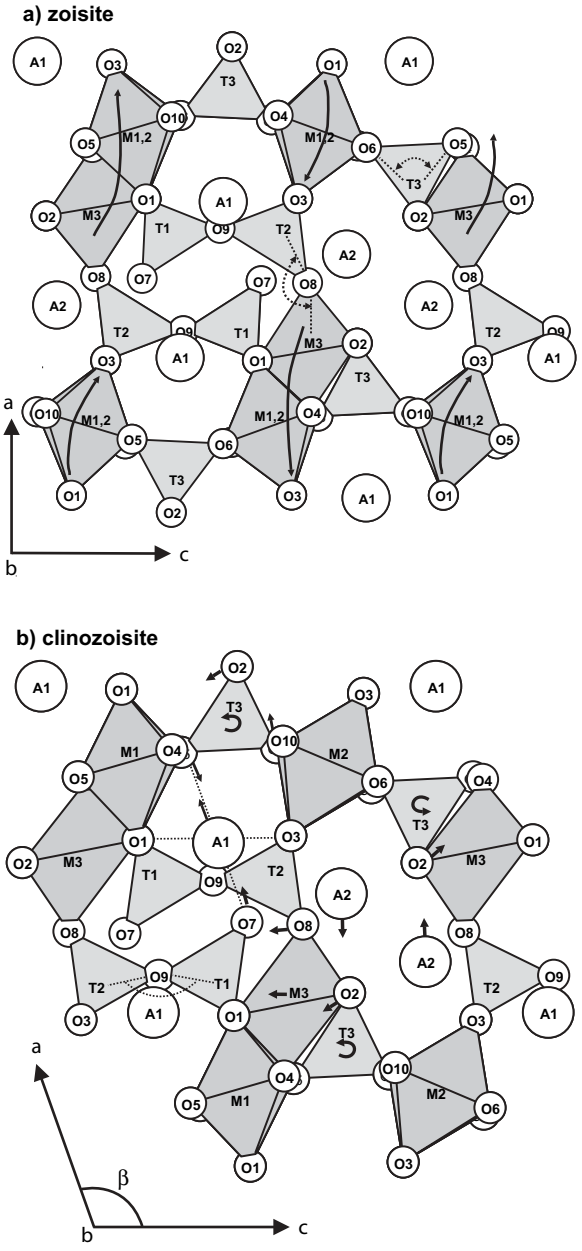

FIGURE 11. (**a**) Displacement of the octahedron blocks in zoisite in response to Sr incorporation; displacement is shown with bold arrows. Laterally linked T3 turn and T1-T2 group is bended by this displacement (dotted arrows). (**b**) Decrease in angle β in clinozoisite, compression of M3 and T3 polyhedra and elongation of the A1-O6 distance in response to Sr-incorporation. Rotation of T3 with O5 toward A1 is combined with a volume decrease in T1 at $X_{Sr} \approx 0.25$, O7-A1 distance relax after that movement (see text).

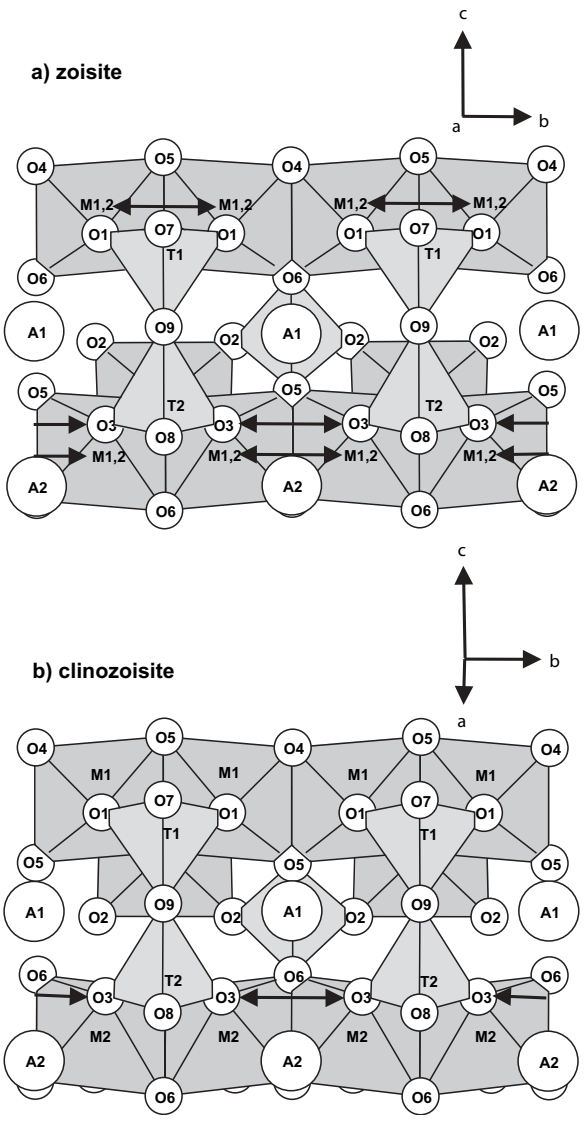

FIGURE 12. Structural changes in the octahedra chain in (**a**) zoisite and (**b**) clinozoisite, projected perpendicular to lattice parameter *b*. Arrows between the O3 atoms show increasing distances along *b* with increasing X_{Sr}. In contrast to the clinozoisite structure, M1 position in zoisite is not a special position, and stretching of the M1-octahedral chain along the b-axis is possible by a small displacement of the central atom with increase of X_{Sr}.

significantly larger than our values. Their positive trend in the average M3 distances (2.03 to 2.09Å) with increasing X_{Mn} is opposite to that with increasing X_{Sr}, i.e., average M3 distances decrease from 2.00 to 1.96 Å and M3 volume decreases (Table A5[1]). The tips (O3-atoms) of the M chain are on a general position and they are strongly displaced by Sr incorporation on A2 (Fig. 12b).

Tetrahedra. The Sr-incorporation in clinozoisite leads to changes also in the geometry of tetrahedral groups. The increase of X_{Sr}^{Czo} causes a torsion of T3 tetrahedra parallel b (Fig. 11b). The O2-T3-O2 angle increases from about 104 to 112° (Table A6[1]) and T3-O2 distances decrease from 1.63 to 1.60 Å. These trends are also opposite to those for Mn-incorporation in piemontite (Nagashima and Akasaka 2004). They observed a continuous decrease in the T1-O9-T2 angle from 156 to 141° with increasing of X_{Mn}, whereas we found an increase from 165 to 171° with a local maximum at about $X_{Sr} \approx 0.25$ with 174°.

The T1 polyhedron volume initially increases with increasing X_{Sr}^{Czo} by the movement of O7 but decreases at $X_{Sr}^{Czo} \approx 0.25$ from 2.51 (Å³) to 2.19 (Å³).

Concluding remarks

The well-known Sr substitution for Ca as it occurs at moderate pressures and temperatures in halides (Brauer and Mueller 1958), carbonates (Chang 1965), phosphates (Bigi et al. 1998), feldspar (Bambauer and Nager 1981), pyroxenes and amphiboles (Najorka et al. 1999) is also possible in the epidote minerals. Much higher Sr concentrations than usually observed in natural epidote minerals were found, and one might speculate that in Sr-rich rocks at low Ca contents even the Sr end-member of zoisite could be found. Changes from CASH to the SrASH system seems to shift the known CASH stability limit of the lawsonite-zoisite transition toward higher temperature and thus expand the stability field of lawsonite. As a first approximation, our data in the SrCASH-system can probably be extended to the $SrCFe^{3+}SH$ and $SrCMn^{3+}SH$-systems with the clinozoisite-epidote and piemontite solid solutions.

Acknowledgments

This work was supported by the DFG with grant no. FR 557/18–1. We thank M. Kreplin for preparing salt pieces, C. Zecha for the polished grain mounts, F. Galbert (ZELMI TU Berlin) for his help with the microprobe analyses, and H. Steigert at the powder XRD.

References cited

Akasaka, M., Zheng, Y., and Suzuki, Y. (2000) Maximum strontium content of piemontite formed by hydrothermal synthesis. Journal of Mineralogical and Petrological Sciences, 95, 84–95.

Anastasiou, P. and Langer, K. (1977) Synthesis and physical properties of piemontite $Ca_2Al_{3p}Mn_p^{3+}(Si_2O_7/SiO_4/O/OH)$. Contributions to Mineralogy and Petrology, 60, 225–245.

Armbruster, T., Bonazzi, P., Akasaka, M., Bermanec, V., Chopin, C., Giere, R., Heuss-Assbichler, S., Liebscher, A., Menchetti, S., Pan, Y., and Pasero, M., (2006) Recommended nomenclature of epidote-group minerals. European Journal of Mineralogy, 18, 551–567.

Bambauer, H.U. and Nager, H.E. (1981) Gitterkonstanten und displazive transformationen synthetischer Erdalkalifeldspäte. I. System $Ca[Al_2Si_2O_8]$-$Sr[Al_2Si_2O_8]$-$Ba[Al_2Si_2O_8]$. Neues Jahrbuch für Mineralogie Abhandlungen, 141, 225–239.

Bigi, A., Falini, G., Gazzano, M., Roveri, N., and Tedesco, E. (1998) Structural refinements of strontium substituted hydroxylapatites. Materials Science Forum, 278, 814–819.

Bonazzi, P. and Menchetti, S. (1995) Monoclinic members of the epidote group: effects of the $Al \leftrightarrow Fe^{3+} \leftrightarrow Fe^{2+}$ substitution and of the entry of REE^{3+}. Mineralogy and Petrology, 53, 133–153.

Bonazzi, P., Menchetti, S., and Palenzona, A. (1990) Strontiopiemontite, a new member of the epidote group, from Val Graveglia, Liguria, Italy. European Journal of Mineralogy, 2, 519–523.

Bonazzi, P., Menchetti, S., and Reinecke, T. (1996) Solid solution between piemontite and androsite-(La), a new mineral of the epidote group from Andros Island, Greece. American Mineralogist, 81, 735–742.

Brastad, K. (1984) Sr metasomatism, and partition of Sr between the mineral phases of a meta-eclogite from Bjørkedalen, West Norway. Tschermaks mineralogische und petrographische Mitteilungen, 34, 87–103.

Brauer, G. and Mueller, O. (1958) Zur Kristallchemie des Strontiumchlorids. Zeitschrift für Anorganische und Allgemeine Chemie, 295, 218–226.

Brown, I.D. and Altermatt, D. (1985) Bond-valence parameters obtained from a systematic analysis of the Inorganic Crystal Structure Database. Acta Crystallographica, B41, 244–247.

Cagliotti, G., Paoletti, A., and Ricci, F.P. (1958) Choice for collimators for a crystal spectrometer for neutron diffraction. Nuclear Instruments, 3, 223–228.

Carbonin, S. and Molin, G. (1980) Crystal chemical considerations on eight metamorphic epidotes. Neues Jahrbuch für Mineralogie (Abhandlungen), 139, 205–215.

Chang, L.L.Y. (1965) Subsolidus phase relation in the system $BaCO_3$-$SrCO_3$, $SrCO_3$-$CaCO_3$ and $BaCO_3$-$CaCO_3$. Journal of Geology, 73, 346–368.

Dollase, W.A. (1968) Refinement and comparison of the structures of zoisite and clinozoisite. American Mineralogist, 53, 1882–1898.

——— (1969) Crystal structure and cation ordering of piemontite. American Mineralogist, 54, 710–717.

——— (1971) Refinement of the crystal structures of epidote, allanite, and hancockite. American Mineralogist, 56, 447–464.

Giuli, G., Bonazzi, P., and Menchetti, S. (1999) Al-Fe disorder in synthetic epidotes: A single-crystal X-ray diffraction study. American Mineralogist, 84, 933–936.

Gottschalk, M. (2004) Thermodynamic Properties of Zoisite, Clinozoisite and Epidote. In A. Liebscher and G. Franz, Eds., Epidotes, 56, p. 83–124. Reviews in Mineralogy and Geochemistry, Mineralogical Society of America, Chantilly, Virginia.

Grapes, R.H. and Hoskin, P.W.O. (2004) Epidote group minerals in low-medium pressure metamorphic terranes. In A. Liebscher and G. Franz, Eds., Epidotes, 56, p. 301–345. Reviews in Mineralogy and Geochemistry, Mineralogical Society of America, Chantilly, Virginia.

Langer, K., Tillmanns, E., Kersten, M., Almen, H., and Arni, R.K. (2002) The crystal chemistry of Mn^{3+} in the clino- and orthozoisite structure types, $Ca_2M_3^{3+}[OH\ O\ SiO_4\ Si_2O_7]$: a structural and spectroscopic study of some natural piemontites and "thulites" and their synthetic equivalents. Zeitschrift für Kristallographie, 217, 563–580.

Larson, A.C. and Von Dreele, R.B. (1987) Generalized structure analysis system. Los Alamos National Laboratory Report.

Lavina, B., Carbonin, S., Russo, U., and Tumiati, S. (2006) The crystal structure of dissakisite-(La) and structural variations after annealing of radiation damage. American Mineralogist, 91, 104–110.

Liebscher, A. and Franz, G. (2004) Physical and Chemical Properties of the Epidote Minerals An Introduction. In A. Liebscher and G. Franz, Eds., Epidotes, 56, p. 1–81. Reviews in Mineralogy and Geochemistry, Mineralogical Society of America, Chantilly, Virginia.

Liebscher, A., Gottschalk, M., and Franz, G. (2002) The substitution $Fe^{(3+)}$-Al and the isosymmetric displacive phase transition in synthetic zoisite: A powder X-ray and infrared spectroscopy study. American Mineralogist, 87, 909–921.

Miyajima, H., Matsubara, S., Miyawaki, R., and Hirokawa, K. (2003) Niigataite, $CaSrAl_3(Si_2O_7)(SiO_4)O(OH)$: Sr-analogue of clinozoisite, a new member of the epidote group from the Itoigawa-Ohmi district, Niigata Prefecture, central Japan. Journal of Mineralogy and Petrology Science. 98, 118–129.

Nagashima, M. and Akasaka, M. (2004) An X-ray Rietveld study of piemontite on the join $Ca_2Al_3Si_3O_{12}(OH)$–$Ca_2Mn_3^{3+}Si_3O_{12}(OH)$ formed by hydrothermal synthesis. American Mineralogist, 89, 1119–1129.

Najorka, J., Gottschalk, M., Franz, G., and Heinrich, W. (1999) Ca-Sr distribution among amphibole, clinopyroxene, and chloride-bearing solutions. American Mineralogist, 84, 596–606.

Nozik, Yu.Z., Kanepit, V.N., Fykin, L.Y., and Makarov, Yu.S. (1978) A neutron-diffraction study of the structure of epidote. Geochemistry International, 15, 66–69.

Pawley, A.R. and Allan, D.R. (2001) A high-pressure study of lawsonite using angle-dispersive powder-diffraction methods with synchrotron radiation. Mineralogical Magazine, 65(1), 41–58.

Poli, S. and Schmidt, M.W. (2004) Experimental Subsolidus Studies on Epidote Minerals. In A. Liebscher and G. Franz, Eds., Epidotes, 56, p. 171–195. Reviews in Mineralogy and Geochemistry, Mineralogical Society of America, Chantilly, Virginia.

Pouchou, J.L. and Pichoir, F. (1984) Un nouveau modèle de calcul pour la microanalyse quantitative par spectrométrie de rayons X. La Recherche Aérospatiale, 3, 167–192.

Robinson, K., Gibbs, G.V., and Ribbe, P.H. (1971) Quadratic elongation: a quantitative measure of distortion in coordination polyhedra. Science, 172, 567–570.

Shannon, R.D. (1976) Revised Effective Ionic Radii and Systematic Studies of Interatomic Distances in Halides and Chalcogenides. Acta Crystallographica, A32, 751–767.

Spandler, C., Hermann, J., and Arculus, R. (2003) Redistribution of trace elements during prograde metamorphism from lawsonite blueschist to eclogite facies; implications for deep subduction-zone processes. Contribution to Mineralogy and Petrology, 146, 205–222.

Tröger, W.E. (1982) Optische Bestimmung der gesteinsbildenden Minerale Teil I.: Bestimmungstabellen. E. Schweizerbart.

Zack, T., Foley, S.F., and Rivers, T. (2002) Equilibrium and disequilibrium trace element partitioning in hydrous eclogites (Trescolmen, Central Alps). Journal of Petrology, 43, 10, 1947–1974.

Zimmermann, R., Heinrich, W., and Franz, G. (1996) Tremolite synthesis from $CaCl_2$-bearing aqueous solutions. European Journal of Mineralogy, 8, 767–776.

Manuscript received June 14, 2006
Manuscript accepted March 2, 2007
Manuscript handled by Paola Bonazzi